Scientific Reports

https://doi.org/10.1038/s41598-026-46873-4

Article in Press

Research on the problem of spatial heterogeneity in row data and generalization capability for landslide susceptibility assessment using the physics-constrained U-net model

Received: 28 January 2026

Accepted: 27 March 2026

Published online: 03 April 2026

Cite this article as: Zhang H. & Deng H. Research on the problem of spatial heterogeneity in row data and generalization capability for landslide susceptibility assessment using the physics-constrained U-net model. *Sci Rep* (2026). https://doi.org/10.1038/s41598-026-46873-4

Heli Zhang & Hongyan Deng

Research on the Problem of Spatial Heterogeneity in Row Data and Generalization Capability for Landslide Susceptibility Assessment using the Physics-constrained U-net Model

Heli Zhang [a], Hongyan Deng [a]

[a] School of Civil Engineering, Southwest Jiaotong University, Chengdu, China

Correspondence:

Hongyan Deng

annedeng@swjtu.edu.cn

Keywords:

Landslide susceptibility

physical constrained U-Net model

spatial heterogeneity in raw data

generalization capability

ABSTRACT

Landslide susceptibility research serves as the primary approach for analyzing the future development of landslides, and could provide the scientific reference for mountainous area development strategic decisions. The accuracy of landslide susceptibility assessment mainly depends on input data and evaluation methods. To address the issues of significant impacts from raw data defects and low spatial resolution in susceptibility assessment results within traditional deep learning evaluation models, this study establishes a physically constrained U-Net model (PCUM). This method selects ten landslide assessment factors, including slope gradient, profile curvature, slope aspect, landform, river distribution density, annual average precipitation, annual average

temperature, fault distribution density, lithology, and seismic intensity. Through adjusting the weights of the model's loss function by imposing explicit physical constraints, the model's performance was ultimately enhanced. A comparison of the model evaluation results before and after applying the constraints is as follows: the AUC value increased from 0.871 to 0.877, the recall increased from 0.884 to 0.891, and the Kappa coefficient rose from 0.597 to 0.605. Meanwhile, the frequency ratio of the very high susceptibility zone increased from 5.64 to 5.80, while that of the very low susceptibility zone decreased from 4.77×10^{-2} to 3.23×10^{-2}. Compared with other deep learning models, the evaluation results of PCUM demonstrate the advantage of maintaining spatial resolution consistent with the original input data, better revealing the spatial characteristics of landslide distribution, and higher accuracy. This study focuses on the southeastern region of Tibet and selects five typical regions to investigate the impact of spatial heterogeneity in raw data on the PCUM. The AUC values of the BP neural network model in the five typical regions are 0.905, 0.930, 0.871, 0.877, and 0.920, respectively, with relatively poor performance in typical regions 3 and 4. The AUC values of the residual neural network model are 0.874, 0.921, 0.915, 0.891, and 0.914, respectively, showing poor performance in typical region 1. In contrast, the PCUM achieves AUC values of 0.923, 0.940, 0.935, 0.915, and 0.899 across the five regions, demonstrating robust performance in all typical areas. The results indicate that the physically constrained U-Net model can effectively handle spatial heterogeneity in raw data and exhibits good generalization capabilities. This study may provide an effective reference for the generalizability research of landslide susceptibility assessment models.

1. Introduction

Under the context of accelerated global climate change, landslide hazards are exhibiting a marked upsurge in both frequency and severity (Brabb, 1991; Petley, 2012; Lin et al., 2022; Duan et al., 2025). As a foundational component of landslide disaster risk management, susceptibility assessment provides essential scientific support for sustainable development strategies in mountainous areas. Notably, the development of robust

susceptibility assessment models constitutes a pivotal prerequisite for achieving high-precision evaluation outcomes, thereby enabling more effective disaster mitigation and land-use.

Landslide susceptibility assessment methods include expert knowledge-driven approaches, physical deterministic modeling methods, and data-driven methods (Huang and Zhao, 2018). Traditional data-driven approaches utilize statistical models like information content and logistic regression to assess landslide susceptibility based on historical records. However, the accuracy of these methods depends extremely on the completeness and precision of historical landslide data on the basis of neglecting the physical relationships among assessment factors (Ciurleo et al., 2017; Reichenbach et al., 2018).

With the advancement of artificial intelligence, machine learning has emerged as one of the primary methods for data-driven landslide susceptibility assessment (He et al., 2024). Compared to statistical models, machine learning demonstrates superior performance and capabilities due to its ability to effectively capture complex nonlinear relationships among landslide assessment factors (Wang et al., 2021; Tsangaratos et al., 2020; Chen et al., 2019; Huang et al., 2023). Transfer learning has also gained significant attention in landslide susceptibility assessment research, as it significantly enhances the generalization ability of models and is particularly applicable in data-scarce regions (Wang et al., 2022; Wang et al., 2025; Wang et al., 2025; Su et al., 2025). However, the application of machine learning in landslide susceptibility assessment still faces two important issues: an extreme dependence on the quality of input data and a reduction in the spatial resolution of evaluation results.

In the realm of data-driven assessment, imbalanced sample sizes and spatial heterogeneity are two critical challenges. Coupled with the tendency of models to focus on numerical correlations among assessment factors while neglecting their underlying physical mechanisms, the accuracy and generalizability of evaluation results are severely compromised. Imbalanced data primarily arises during dataset creation. In reality,

landslide areas usually occupy only a small portion of the study area, making it difficult to maintain a balance between the number of landslide samples and non-landslide samples. This inevitably leads to the model extracting more features from one class of samples while inadequately learning features from the other, ultimately resulting in reduced model performance and lower generalization ability. Current approaches to addressing data imbalance in research primarily focus on improving the dataset through data augmentation and enhanced sampling methods. Because landslide susceptibility assessment factors often include non-continuous data such as lithology and landform classifications, the use of data augmentation methods is restricted. Wei et al. processed the discrete assessment factor of lithology by using the TRIGRS model to convert it into a continuous safety factor. They also adopted relatively conservative geometric transformation methods, applying special angles such as 90°, 180°, and 270° for sample rotation (Wei et al., 2021). There is relatively more research focused on the improvement of sampling methods. Some scholars continuously adjust the sample ratio to find a balance between making the data reflect reality and ensuring adequate model learning, ultimately improving model performance (Huang et al., 2024). Some scholars use other models to screen existing samples, improving the quality and balance of the dataset, thereby enhancing the accuracy of the results. (Wang et al., 2024; Gupta & Shukla, 2023). Some scholars generate high-quality new samples using other models to supplement and correct the dataset (Han & Semnani, 2025; Jiang et al., 2025). However, improving and optimizing the dataset alone is insufficient; the model's inherent capacity to handle this issue must also be enhanced.

The study area covers 334,200 km², significantly larger than that of related studies, making the spatial heterogeneity of the dataset a non-negligible factor. Spatial heterogeneity data stems from the inherent spatial variability of landslides and systematic errors during geological surveys. There are two reasons: one is that the mechanisms and main factors of landslides show spatial heterogeneity in different regions, which leads to the overfitting of models and the decrease in accuracy of assessment results (Sun et al., 2023; Zhao et al., 2024). Another one is the big difference in landslide investigation depth

between remote areas and important development zones, which can amplify the spatial heterogeneity of the data. Spatial heterogeneity of data imposes higher demands on models, which must possess strong generalization capabilities to fully capture the characteristics of landslides with diverse types and mechanisms. It is the basis to obtain reliable susceptibility assessments within the evaluation area.

Finally, traditional machine learning models reduce the spatial resolution of landslide susceptibility assessment results, diminishing their practical value. Machine learning models rely on sample data to efficiently classify and predict sample labels. During the feature learning process, they tend to focus more on whole abstract features while gradually discarding local detailed features. In landslide susceptibility assessment, samples are formed by merging data obtained from multiple evaluation factors through a sampling window. Each data point contains multiple pixels, and the geographic scale corresponding to the sampling window is larger than the spatial resolution of the original data. However, machine learning models can only predict the overall probability of landslides for the input samples and cannot assess the landslide risk for each pixel within the sample. This ultimately results in the spatial resolution of the assessment results being reduced to the spatial scale of the sampling, which is lower than the original resolution of the input data.

To tackle the common challenges in landslide susceptibility assessment—namely, sample imbalance, spatial heterogeneity due to the extensive study area (333,700 km^2), and the loss of spatial resolution inherent in traditional machine learning methods—this study adopts a U-Net model incorporating explicit physical constraints. The U-Net model is a semantic segmentation model, with a skip-connection framework that preserves image dimensions while retaining the spatial feature details of factor data in landslide evaluation, that enhances assessment accuracy without compromising the spatial resolution of susceptibility evaluation results. Subsequently, the sample weights in the loss function are adjusted to increase the model's attention to under-represented samples, ensuring adequate learning. Additionally, physical constraints are introduced into the loss function to optimize the model training process by penalizing unreasonable predictions. Finally, the

landslide susceptibility assessment results achieve a fine and accurate match with the spatial resolution of the assessment factors, while also demonstrating stronger generalization ability.

2. Study Area

The study area comprises Lhasa, Zedang, Nyingchi, and Qamdo in southeastern Tibet, covering a total area of approximately 334,200 square kilometers (Figure 1, spatial resolution: 30m). Situated at the junction of the Indian and Eurasian tectonic plates, the prominent disaster environmental characteristics of the study area are intense tectonic activity, steep slopes, and extreme climatic conditions, the high incidence of landslide disasters has become inevitable. Landslide disasters are frequent and concentrated in the study area. According to historical disaster point data, landslides are mainly concentrated in areas with complex geological conditions, such as the Great Bend of the Yarlung Zangbo River, the "Three Parallel Rivers" area in eastern Tibet (the Nujiang, Lancang, and Jinsha rivers), and the Lhasa River basin. Moreover, the complex characteristics of disaster environments contribute to the diversity and variability of landslide hazards. Therefore, the evaluation model must possess robust generalization capabilities. Such capabilities are essential for it to learn the characteristics of different landslide types and provide reliable results in various regions.

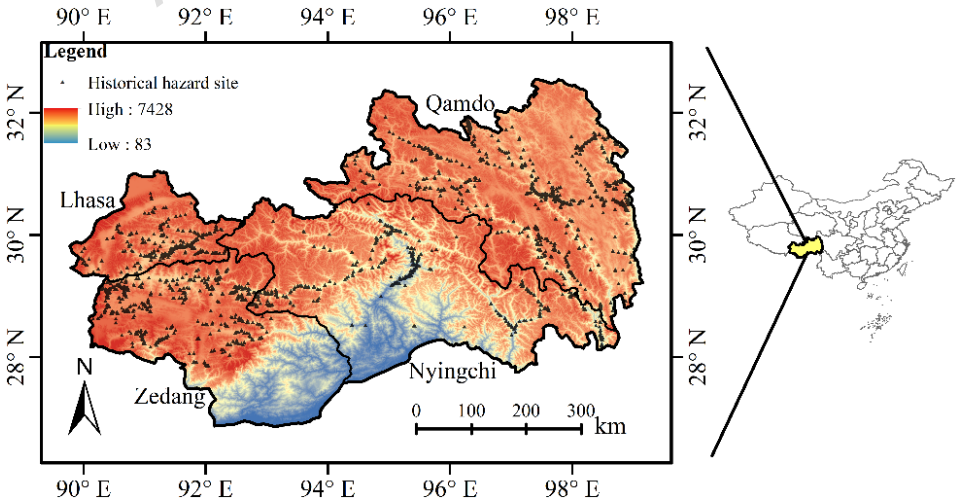

Figure 1: Study area. Maps were generated using ArcGIS Desktop 10.6.1 (Build 9270, https://www.esri.com).

3. Database and method

3.1. Research Data

3.1.1. Data Collection

The landslide disasters result from the interaction of multiple assessment factors. The factors for landslide susceptibility assessment must encompass both main conditions and triggering factors (Zhong et al., 2024; Qian et al., 2025). In order to embody the comprehensiveness of landslide susceptibility assessment factors, this study collects data from four domains: topography and landforms, hydrometeorology, geology, and land cover. A total of 10 landslide susceptibility assessment factors were compiled: slope gradient, profile curvature, slope aspect, landform, river distribution density, annual average precipitation, annual average temperature, fault distribution density, lithology, and seismic intensity. The data sources for this study are shown in Table 1, where the spatial resolution of the raster data has been annotated, and the temporal resolution of the rainfall and temperature data is annual.

Table 1 Data sources for historical hazard sites and landslide susceptibility evaluation factors

Data	Data Source	Original Spatial Resolution
Historical hazard site data	http://www.gisrs.cn/	\
Elevation data	https://panda.copernicus.eu/panda	30m
Topographic Data	Topographic Map of China (1:4,000,000)	\
River Data	https://www.openstreetmap.org	\
Rainfall data	https://data.tpdc.ac.cn	1000m
Air temperature data	https://data.tpdc.ac.cn	1000m

Fault data	https://news.ceic.ac.cn/	\
Lithological data	https://www.cgs.gov.cn/	\
Seismic Intensity Zoning Data	https://www.gb18306.net/	\

3.1.2. Data Processing

The disaster point data is point vector data, with a total of 1,955 locations. Slope gradient, profile curvature, and aspect data were derived from elevation data through GIS analysis, with a spatial resolution of 30m. Topographic, lithology, and seismic intensity are vector data. They were assigned values and organized into raster data with a spatial resolution of 30m. River distribution density and fault distribution density were derived from their respective vector data through line density analysis in ArcGIS, with a spatial resolution of 30m. Annual average precipitation and annual average temperature were converted to a spatial resolution of 30m through raster interpolation in ArcGIS. Finally, all landslide assessment factors adopt the WGS-84 coordinate system with a spatial resolution of 30 meters, as shown in Figure 2.

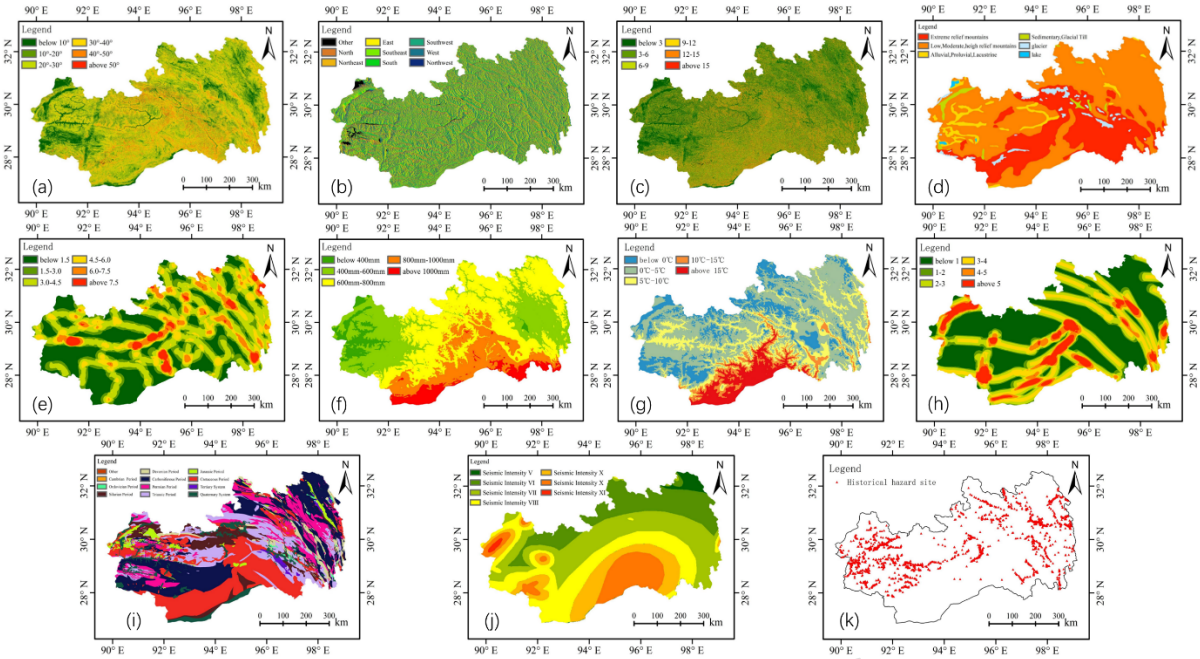

Figure 2: Historical hazard site and factors distribution in the study area: (a) slope gradient; (b) profile curvature; (c) slope aspect; (d) topographic; (e) river distribution density; (f) annual average precipitation ; (g) annual average temperature; (h) fault distribution density; (i) lithology; (j) seismic intensity; (k) Historical hazard site. Maps were generated using ArcGIS Desktop 10.6.1 (Build 9270, https://www.esri.com).

Landslide assessment factors often exhibit correlations, then there is a risk of overfitting the model (Li et al., 2025; Kong et al., 2025; Shi et al., 2025). Because of the differences among various landslide assessment factors in dimensionality and variability, the model training becomes difficult and complex. Therefore, correlation screening and preprocessing of landslide assessment factors are indispensable. This study conducted Pearson correlation analysis on landslide susceptibility assessment factors, where the absolute magnitude of the correlation coefficient represents the strength of association between factors. The Pearson correlation formula is as follows:

$$r_{XY} = \frac{cov(XY)}{s_X s_Y}$$

$$cov(XY) = \sum_{i=1}^{n} (x_i - \bar{X})' (y_i - \bar{Y})$$

Where r_{XY} is the Pearson correlation coefficient between variable X and variable Y. $cov(XY)$ is the covariance between variable X and variable Y.

The results of the correlation analysis of landslide susceptibility assessment factors are shown in Figure 3. Ten factors for landslide susceptibility assessment are independent of each other. For discrete landslide susceptibility factors (slope aspect, landform, lithology, and seismic intensity, totaling 4 types), integer values starting from 1 were assigned to different classification types. For continuous landslide susceptibility factors (slope gradient, profile curvature, river distribution density, annual average precipitation, annual average temperature, and fault distribution density, totaling 6 factors), normalization was performed to enhance model performance and accelerate training speed.

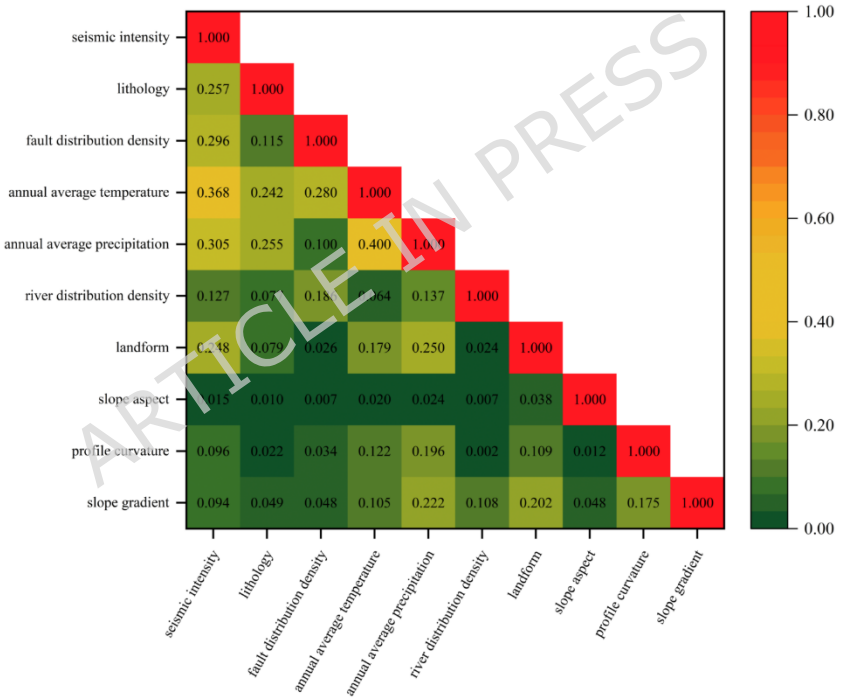

Figure 3: Correlation analysis results of landslide susceptibility assessment factors.

3.2. Research Methods

3.2.1. Basic Ideas and Innovations

Traditional machine learning-based evaluation models can only perform label classification on samples, but are unable to identify landslide risks within the internal regions of samples

in detail. As a result, the spatial resolution of the model evaluation outcomes is reduced to the spatial scale of sample sampling, which is lower than the spatial resolution of the original input data. Common approaches for addressing sample imbalance—such as data augmentation, generating new samples, and improving sampling methods—only modify the dataset, while overlooking the model's inherent adaptability to such issues. Additionally, the large extent of the study area introduces significant spatial heterogeneity. Therefore, this paper conducts a landslide susceptibility assessment based on the U-Net model, incorporating weight adjustment and physical constraints into the loss function. The skip connections, upsampling structure, and corresponding decoding process of the U-Net model can preserve the spatial detail features of landslide assessment factors, ultimately improving the spatial resolution and practical application value of the evaluation results. Considering the common problem of sample imbalance, adjusting the weights of different labels in the cross-entropy function can increase the model's attention to minority samples, ensuring thorough learning. Finally, the physical constraints on the loss function can optimize the model's training process, ensuring timely and effective adjustments, thereby improving the accuracy of the evaluation results. The process for conducting landslide susceptibility assessments is shown in Figure 4.

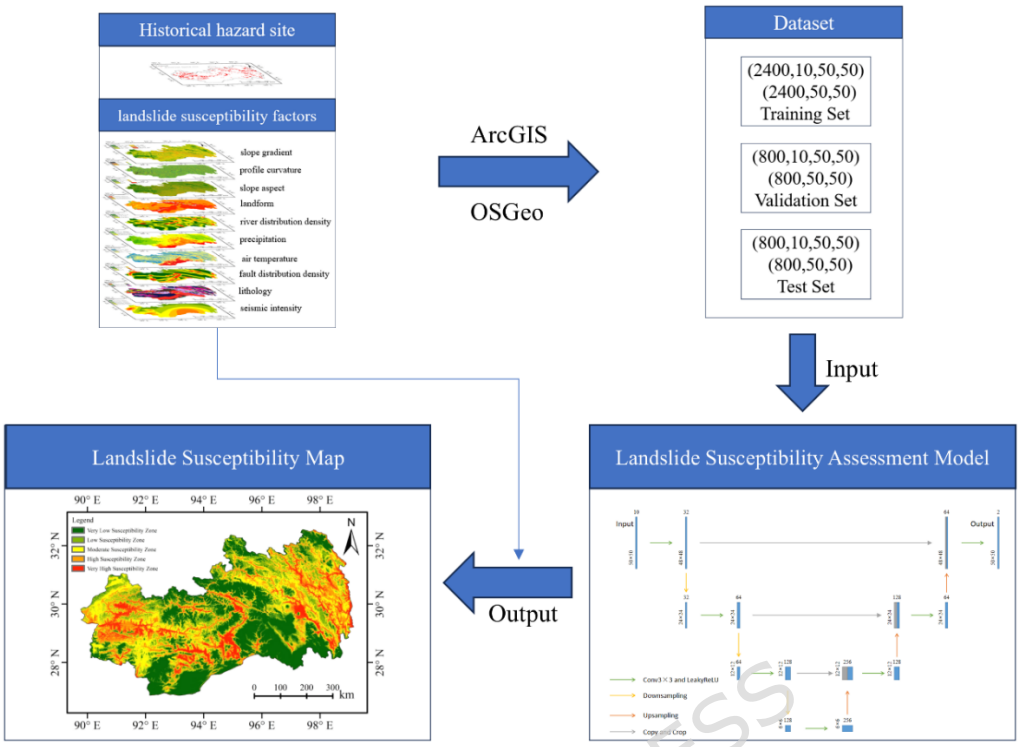

Figure 4: Landslide susceptibility assessment flowchart. Maps were generated using ArcGIS Desktop 10.6.1 (Build 9270, https://www.esri.com).

3.2.2. Dataset Production

The U-Net model requires pixel-level classification labels. Some scholars extract pixel points that best represent the environmental characteristics of landslide occurrences from landslide polygons, measure the reliability of each sample through the similarity of environmental factors, and perform screening, ultimately improving the accuracy of the evaluation results (Hong et al., 2024). As the landslide catalog data in this study is point vector data, the traditional landslide neighborhood method was applied: pixels within the buffer range were classified as landslide areas, and those outside as non-landslide areas. The buffer radius is determined by the landslide scale recorded in the landslide catalog data: 600 m for giant, 500 m for large, 400 m for medium, and 300 m for small or unrecorded landslides.

Subsequently, OSGeo was used to sample the original data containing landslide areas with a 1500m × 1500m rectangle, obtaining a total of 2,235 samples (as the sampling

radius is larger than the buffer radius, these samples include both landslide and non-landslide areas). These samples are located relatively close to the landslide disaster points and contain more landslide-related features. In order to enrich the non-landslide features, random sampling was conducted in areas far from the landslide disaster points using the same method (these samples contain only non-landslide areas), yielding 1,756 samples. Ultimately, the model dataset was constructed. A statistical analysis of the completed dataset shows that the ratio of landslide areas to non-landslide areas is approximately 1:5. To perform cross-validation of the model, the dataset was randomly divided into a training set (60%), a validation set (20%), and a test set (20%). The schematic diagram of the model sample is shown in Figure 5.

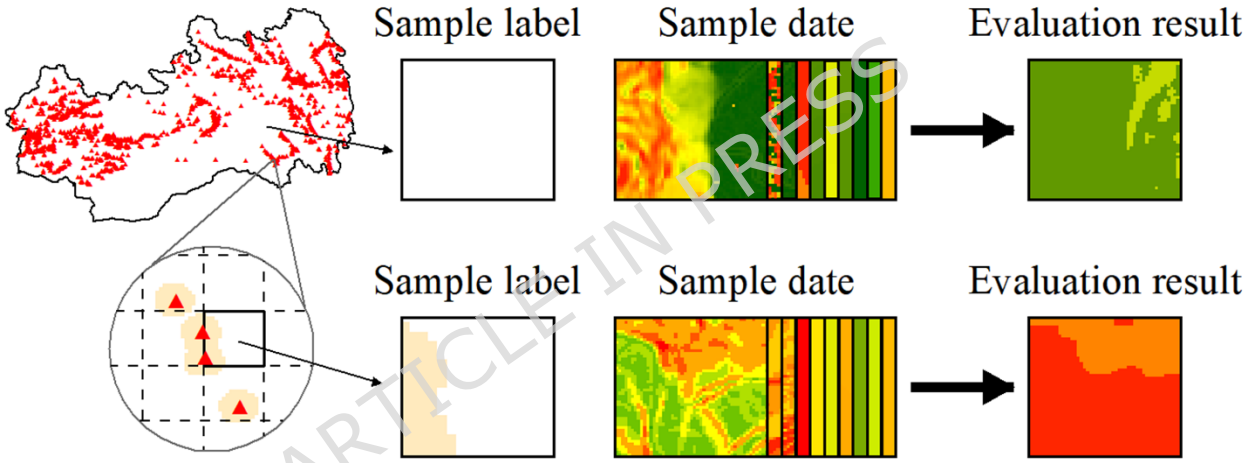

Figure 5: Model Sample Examples. Maps were generated using ArcGIS Desktop 10.6.1 (Build 9270, https://www.esri.com).

3.2.3. Model Construction

The U-Net model consists of an encoder-decoder architecture and skip connections, enabling high-precision pixel-level predictions. The encoder reduces the spatial resolution of images and increases the number of feature channels, ensuring the model can fully learn the features of the images. The decoder performs upsampling on the features learned by the model, gradually restoring the image's spatial resolution. The skip-connection architecture enables the model to preserve spatial details in images while mitigating gradient vanishing, thereby enhancing training efficiency. The model structure of this

paper is shown in Figure 6. This encoder performs image feature extraction using a convolutional layer with a 3×3 kernel and the LeakyReLU activation function. The LeakyReLU function is a variant of the ReLU function that prevents “neuron death” and enhances training process stability. For improved model learning capacity, the encoder replaces standard max/average pooling by leveraging a convolutional layer with a 2×2 kernel. The upsampling module in the decoder first increases the image resolution via nearest interpolation and then applies a 1×1 convolution to reduce the number of feature channels. Leveraging the encoder's high-level features, it progressively restores the spatial resolution and details of the image. The skip connections operate by copying and concatenating corresponding encoder and decoder feature maps along the channel dimension. This mechanism serves to retain crucial spatial detail information from the image. To prevent overfitting and improve generalization, the model incorporates BatchNorm and Dropout layers after the convolutional layers, with the former performing normalization and the latter randomly dropping neurons during training.

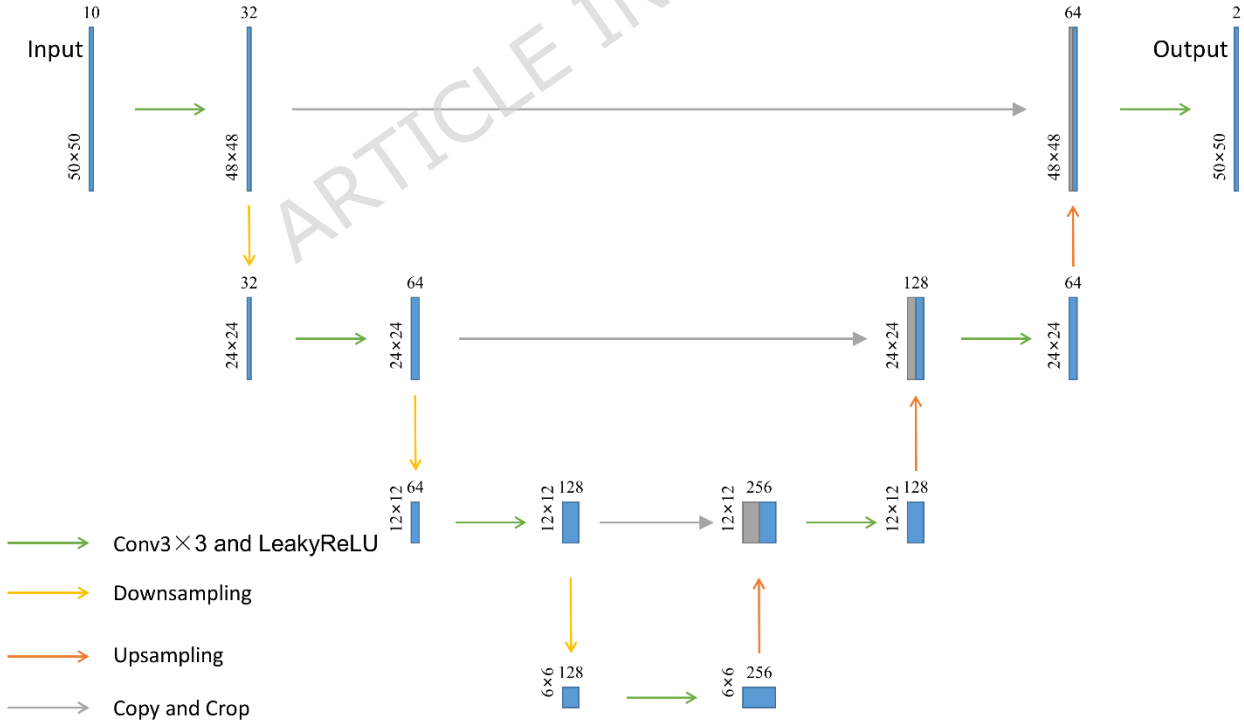

Figure 6: Schematic diagram of the U-Net model for landslide susceptibility analysis.

3.2.4. Model Adjustment and Constraints

The model's loss function consists of two parts: the base loss function and the physical constraint loss function. The formula is as follows:

$$loss = loss_{bce} + loss_{phy} \tag{1}$$

Where $loss_{bce}$ is the base loss function, $loss_{phy}$ is the physical constraint loss function.

The base loss function of the model employs the Cross-Entropy function. To address the data imbalance issue within the model, the weights for landslides and non-landslides in the Cross-Entropy function are set to 5.0 and 1.0 respectively, thereby enhancing the model's learning of features specific to landslide areas.

The physical constraints of the model are implemented through a landslide early warning system. When the cumulative rainfall in landslide-prone areas exceeds the critical rainfall threshold, a landslide warning is triggered, indicating an increased risk of landslides (Emberson et al., 2020). Experts have analyzed and summarized landslide early warning systems, concluding that a 7-day period is a commonly used and effective time window for characterizing soil and hydrological conditions (Guzzetti et al., 2020). The 7-day cumulative critical rainfall threshold has been adopted by multiple relevant systems worldwide (Piciullo et al., 2018). To ensure program stability during operation, the model's physical constraints do not directly employ the commonly used landslide hazard index (the ratio of critical rainfall to actual rainfall). Instead, the safety factor for the region is defined as follows:

$$F_s = \frac{1}{1 + k \times R_7} \tag{2}$$

$$k = \frac{1}{R_c} \tag{3}$$

Where F_s is the regional safety factor, with a value less than 0.5 triggering a high-risk landslide warning. k is a regional coefficient. R_c is the critical rainfall threshold derived from historical landslide events in the target area. R_7 is the 7-day cumulative rainfall.

Calculate regional coefficients for different areas based on varying topography. The critical rainfall threshold (R_c) is derived from the distribution of 7-day cumulative rainfall (R_7) preceding historical landslide events. Relevant studies suggest that the 95th percentile statistically represents "extreme rainfall events," which can ensure the hit rate while controlling the false alarm rate (Emberson et al., 2020). Therefore, the 95th percentile of the 7-day cumulative rainfall preceding historical landslide events is used as the critical rainfall threshold. Considering that the specific occurrence time of landslide disasters is not recorded and the corresponding accurate antecedent rainfall is difficult to obtain, the 7-day cumulative rainfall (R_7)was calculated based on the annual rainfall of the target area combined with local meteorological data, using the following formula:

$$R = a \times b \times \frac{7}{n} \times R_{annual} \quad (4)$$

Where R_{annual} is annual precipitation, n is the number of rainy days in the monsoon season, a is the rainfall concentration index, representing the proportion of rainy season rainfall in the annual rainfall. b is the short-term intensity factor, representing the ratio of the maximum rainfall to the average rainfall during the rainy season. The specific values for these parameters are provided in Table 2. Based on the varying topography of the target areas, regional coefficients were calculated using historical landslide data. The results are presented in Table 3.

Table 2 Target area 7-Day cumulative rainfall calculation parameters table

Region	Climate zone	α	β	monsoon season
Nyingchi	Southeastern Tibet Humid Region	0.80	2.5	May to September
Nedong	Southern Tibet Semi-Arid River Valleys	0.85	2.2	June to September
Lhasa	Southern Tibet Temperate Semi-Arid Plateau	0.90	2.0	June to September

Qamdo	Eastern Tibet Humid to Semi-Humid Alpine Gorges	0.75	2.3	May to September

Table 3 Calculation results of regional coefficients for different topographic classifications

topography	k
lakes	0.0119
glaciers	0.0263
plains or terraces formed by sedimentary or glacial deposits	0.0260
plains or terraces formed by alluvial, fluvial, or lacustrine deposits	0.0225
mountainous	0.0129

Ultimately, during model training, the loss function is adjusted based on the predicted probability of landslides occurring and whether the area has triggered a landslide warning. Excessively strong physical constraints can make it difficult for the model to converge. Therefore, constraints are only applied to dangerous situations where a high-risk landslide warning is triggered, but the model predicts safety. When the model predicts a low probability of landslides (below 0.15) but the area's safety factor falls below 0.5, triggering a high-risk landslide warning, the model's loss function is appropriately amplified to penalize unreasonable predictive behavior. The formula is as follows:

$$loss_{phy} = \lambda \times H(p, F_s) \times sigmoid(1 - F_s) \tag{5}$$

Where λ is the physical constraint strength coefficient. $H(p, F_s)$ is an indicator function defined as follows: $H(p, F_s) = 1$ when the model predicts a low probability of landslide occurrence ($p < 0.15$) and a high-risk landslide warning is triggered ($F_s < 0.5$), and $H(p, F_s) = 0$ otherwise.

4. Results

4.1. Evaluation results

The physical constraint strength coefficient for the model's loss function was set to 0.1, with a learning rate of 0.0001, undergoing 1000 training epochs. Based on the model's performance on the validation dataset, the parameters from epoch 537 were selected as the final parameters. At this point, the validation dataset achieved an accuracy of 91.73% with an average loss function of 9.00×10^{-3}; the training dataset achieved an accuracy of 91.62% with an average loss function of 9.48×10^{-3}. The test dataset achieved an accuracy of 92.31% with an average loss function of 9.30×10^{-3}. (Figure 7)

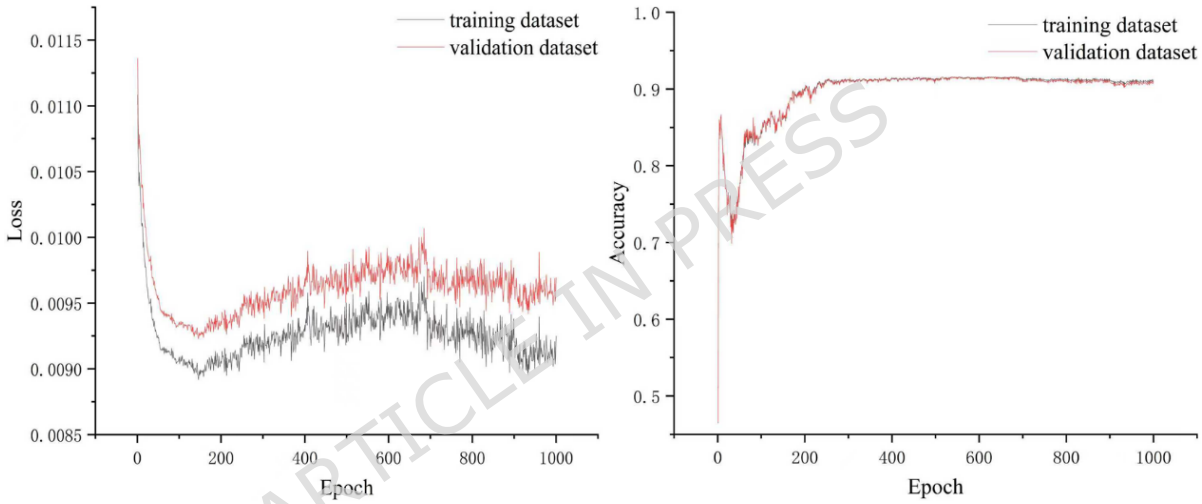

Figure 7: Average loss function and accuracy during model training.

Input the landslide susceptibility factors for the study area into the trained landslide susceptibility model. Apply the output to a SoftMax function to obtain the landslide probability data for the study area. Set threshold values based on area proportions to allocate the regional area distribution across high-, medium-, low-, and very low-susceptibility zones at 10%, 20%, 20%, 20%, and 30%, respectively. This yields the final landslide susceptibility evaluation results for the target area. The results of the landslide susceptibility assessment are shown in Figure 8.

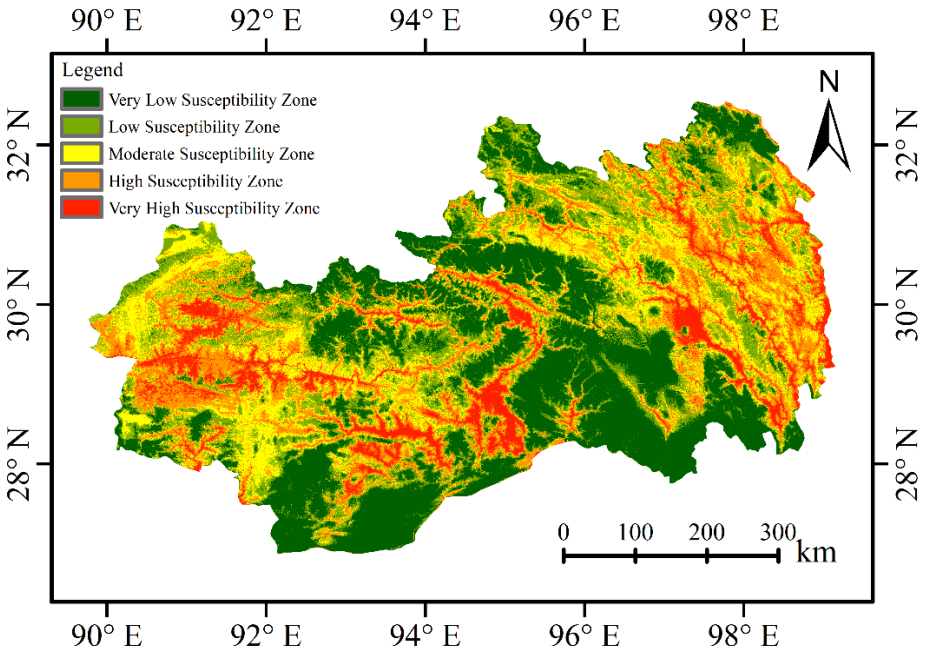

Figure 8: Landslide prone area evaluation results. Maps were generated using ArcGIS Desktop 10.6.1 (Build 9270, https://www.esri.com).

High-risk landslide zones within the study area are primarily concentrated in regions with complex geological conditions. Representative examples include the Yarlung Zangbo River basin, the Three Parallel Rivers region (Nujiang, Lancang, and Jinsha rivers), and the Lhasa River basin. The results of the landslide susceptibility assessment generally align with the spatial distribution patterns of landslide disaster sites in Figure 2.

4.2. Model validation

The ROC curve is the most commonly used method for evaluating the accuracy of landslide susceptibility assessments. The AUC value (area under the ROC curve) effectively reflects model performance and remains unaffected by variations in threshold values (Frattini et al., 2010). Comparing model performance before and after constraint application, the Cross-Entropy function of the unconstrained U-Net model used for comparison assigns weights of 1.0 and 4.0 to non-landslides and landslides, respectively (adjusting to 1.0 and 5.0 resulted in unstable model training, highly fluctuating accuracy curves, and significant discrepancies between training and validation sets, indicating severe overfitting). All other parameters and structures remain identical. Using ArcGIS,

randomly sample non-disaster points within the target area equal in number to historical disaster points, plot the model's ROC curve, and calculate the AUC value (Figure 9).

The AUC values for landslide susceptibility evaluation using U-Net before and after physical constraints were 0.8707 and 0.8765, respectively. By adjusting the Cross-Entropy function weights of the U-Net model and applying physical constraints, the model effectively ensured thorough learning of landslide and non-landslide features. Simultaneously, penalizing unreasonable prediction behaviors enhanced the model's ability to handle defects in raw data, thereby improving overall accuracy.

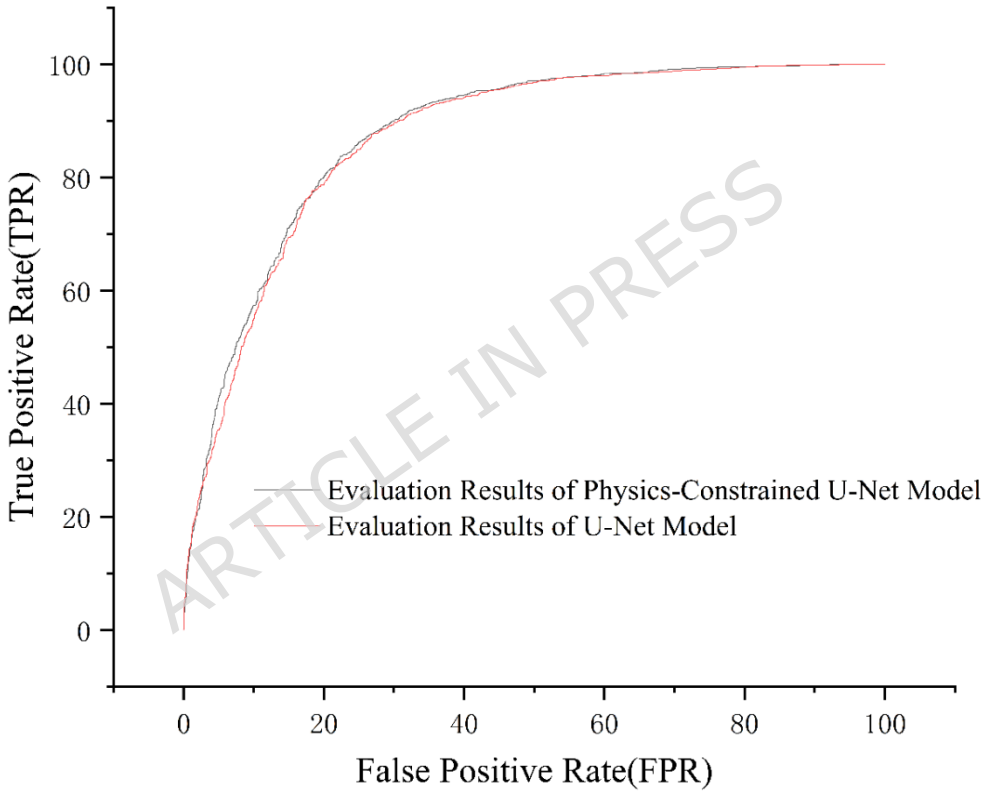

Figure 9: ROC curves for constrained and unconstrained U-Net models.

Historical disaster point validation is the most direct and reliable method for evaluating landslide susceptibility assessment results, as it can verify the accuracy and reasonability of the outcomes. By importing the evaluation results of the model before and after adjusting the constraints into ArcGIS and overlaying them with historical disaster point data from the study area, the proportion of disaster points and frequency ratio for each

susceptibility class in the landslide susceptibility assessment results can be obtained. The results are shown in Table 4.

Frequency ratio is defined as the ratio of the proportion of historical disaster points to the proportion of area for each susceptibility class. The frequency ratios of the evaluation results both before and after the application of physical constraints satisfy the following order: very high susceptibility zones > high susceptibility zones > medium susceptibility zones > low susceptibility zones > very low susceptibility zones. However, after applying physical constraints, the frequency ratio of the very high susceptibility zone increased from 5.64 to 5.80, while that of the very low susceptibility zone decreased from 4.77×10^{-2} to 3.23×10^{-2}. This indicates that the introduction of physical constraints has made the evaluation results more reasonable and accurate.

Table 4 Comparison of disaster point distribution

Model	Susceptibility zones	Disaster point proportion	Area proportion	Frequency ratio
U-Net model	very low	1.43%	30%	4.77×10^{-2}
	low	2.20%	20%	1.10×10^{-1}
	medium	7.98%	20%	3.99×10^{-1}
	high	32.02%	20%	1.60
	very high	56.37%	10%	5.64
Physics-Constrained U-Net Model	very low	0.97%	30%	3.23×10^{-2}
	low	2.45%	20%	1.23×10^{-1}
	medium	7.52%	20%	3.76×10^{-1}
	high	31.10%	20%	1.56
	very high	57.96%	10%	5.80

Recall and the Kappa coefficient are crucial for validating landslide susceptibility results. The former measures the model's performance in addressing high-consequence underprediction events (false negatives), while the latter assesses the consistency between the evaluation results and the actual spatial distribution of landslides. The formulas for recall and the Kappa coefficient are shown as follows.

$$Recall = \frac{TP}{TP + FN} \tag{6}$$

$$Kappa = \frac{P_a - P_e}{1 - P_e} \tag{7}$$

$$P_a = \frac{TP + TN}{N} \tag{8}$$

$$P_e = \left(\frac{TP + FP}{N} \cdot \frac{TP + FN}{N}\right) + \left(\frac{FN + TN}{N} \cdot \frac{FP + TN}{N}\right) \tag{9}$$

The evaluation results of the two models, along with the statistics of landslide and non-landslide points, are summarized in Table 5. Based on the calculations, the recall and Kappa coefficient of the model before physical constraints were 0.884 and 0.597, respectively. After applying constraints, these values increased to 0.891 and 0.605, respectively. This indicates that the physical constraints improved the performance of the evaluation results.

Table 5 Comparison of model prediction results

Model	Prediction results	landslide points	non-landslide points
U-Net model	landslide points	TP=1728	FP=560
	non-landslide points	FN=227	TN=1395
	landslide points	TP=1741	FP=559

Physics-Constrained U-Net Model	non-landslide points	FN=214	TN=1396

A summary of the model evaluation results before and after applying constraints is as follows: the AUC value increased from 0.871 to 0.877, the recall increased from 0.884 to 0.891, and the Kappa coefficient increased from 0.597 to 0.605. Meanwhile, the frequency ratio of the very high susceptibility zone increased from 5.64 to 5.80, while that of the very low susceptibility zone decreased from 4.77×10^{-2} to 3.23×10^{-2}. The improvement in multiple indicators suggests that the weight adjustment of the model's loss function and the physical constraints played a positive role in enhancing the accuracy of the evaluation results.

5. Discussion

5.1. Previous Research

Machine learning is widely applied in the field of landslide susceptibility assessment. The LWL-RS-ADT model performed well in Yongxin County, but experts also found that the model is sensitive to parameters, which may easily lead to overfitting (Hong, 2023). The MB-MLP model was stable and effective in Yanshan County, and experts found in their research that the model's generalization ability is influenced by various factors, including model parameters and complexity (Hong, 2023). When the study area is large and the original data suffers from issues such as sample imbalance and spatial heterogeneity, the generalization ability of the model becomes crucial. It must ensure that the model achieves high accuracy across all regions, avoiding overfitting, where it performs well in some areas but shows reduced accuracy in others. Furthermore, the essence of machine learning is to achieve efficient label classification based on sample data. Traditional models can predict landslide risk at the sample level but are unable to identify risks within internal regions at a detailed level. As a result, the spatial resolution of the model's evaluation outcomes is

reduced to the spatial scale of sample sampling, which is lower than the spatial resolution of the original input data. Therefore, the physically constrained U-Net model is employed for comparison with other commonly used models, evaluating both spatial resolution and generalization capabilities.

5.2. The assessment results of BPNN and ResNet models

The assessment results of the physics-constrained U-Net model were benchmarked against those of the Backpropagation (BP) Neural Network and the Residual Neural Network (ResNet). The architectures and assessment results of these comparative models are presented in Figure 10.

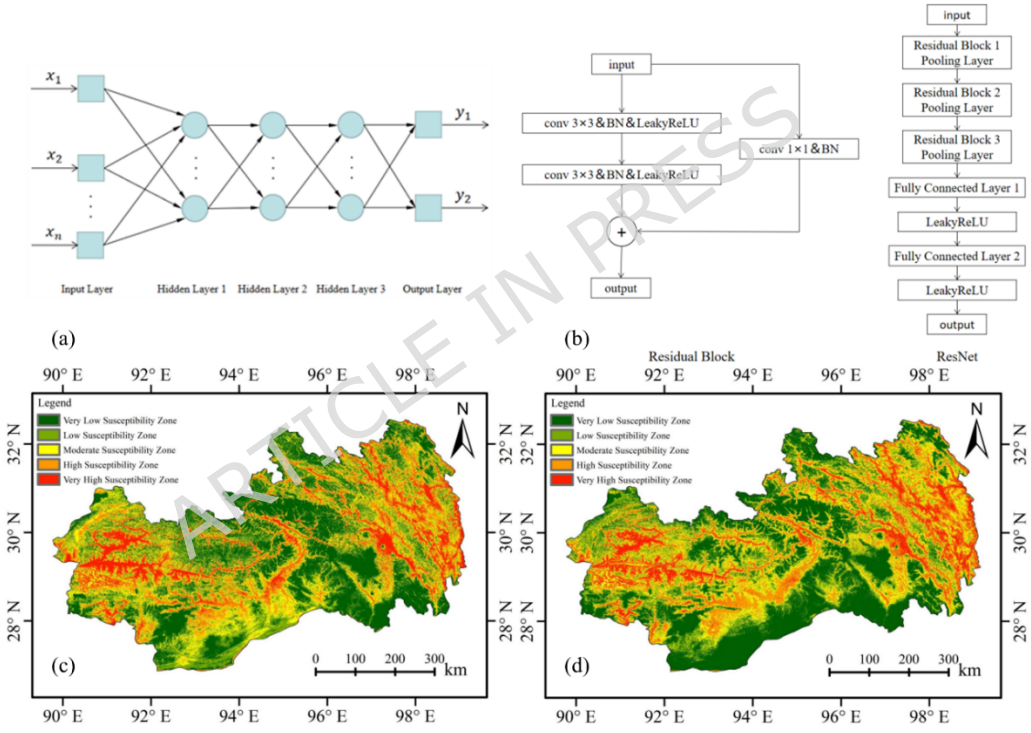

Figure 10: Structures and evaluation results of other common deep learning models:(a) BP Neural Network Model;(b) Residual Neural Network Model;(c) Results of BP Neural Network Model;(d) Results of Residual Neural Network Models. Maps were generated using ArcGIS Desktop 10.6.1 (Build 9270, https://www.esri.com).

The landslide susceptibility assessment model based on the BP neural network consists of one input layer, three hidden layers, and one output layer. It uses the Sigmoid function

as the activation function, and a Dropout layer is added to the model. The landslide susceptibility assessment model based on the residual neural network passes through three residual blocks and pooling layers, followed by two fully connected layers and the LeakyReLU activation function to obtain the final output. The residual path of each residual block includes structures such as a convolutional layer with a 3×3 kernel, a batch normalization layer, and the LeakyReLU activation function. Their learning rates are set to 0.00002 and 0.00005, respectively. The model parameters in this study were selected through multiple rounds of debugging. Conservative parameter choices can lead to slow convergence or severe overfitting, causing the model to become trapped in local optima. Conversely, aggressive parameter choices may result in significant fluctuations in the loss function and failure to converge.

5.3. Comparison of model detail levels

The skip-connection architecture of the U-Net model enables it to preserve spatial details in input data while performing classification, ultimately achieving the semantic segmentation task of assigning category labels to each pixel. In contrast, both the BP neural network model and the residual neural network model progressively discard spatial details during downsampling, retaining only global features. Consequently, they can only accomplish the task of assigning labels to samples. The spatial resolution of input data for landslide susceptibility assessment is 30m. Due to the presence of upsampling layers and skip connections, the U-Net model is able to decode high-level features and recover the detailed features lost during downsampling, enabling pixel-level landslide risk prediction. As a result, the spatial resolution of the final evaluation results is consistent with that of the original input data, also at 30 meters. Both the BP neural network model and the residual neural network model can only predict landslide risk at the sample level. Since the samples geographically correspond to a 600m × 600m rectangle, the spatial resolution of their evaluation results is reduced to 600m (Table 4).

Table 6 Comparison table of spatial resolution in model evaluation results

Name	Landslide Assessment factors	Evaluation Results of BP Neural Network Model	Evaluation Results of Residual Neural Network Models	Evaluation Results of the Physically Constrained U-Net Model
Spatial resolution	30m	600m	600m	30m

Using the Great Bend of the Yarlung Zangbo River as an example, we evaluate and compare the model's performance in typical regions, as shown in Figure 11. The U-Net model preserves the spatial detail features of landslide susceptibility assessment factors through its skip-connection structure, ultimately yielding landslide susceptibility assessment results with high spatial resolution. This approach better reveals the spatial characteristics of landslide hazard distribution and demonstrates greater precision.

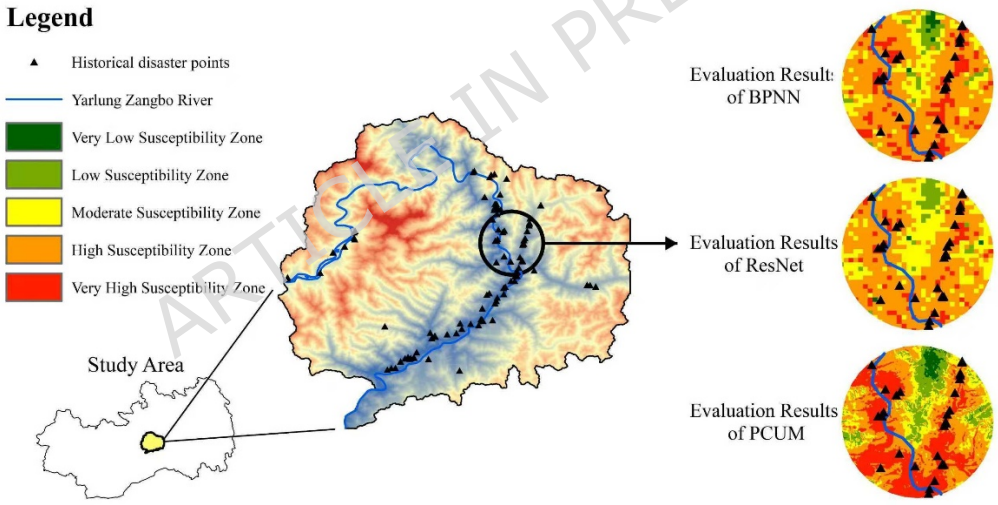

Figure 11: Structures and evaluation results of BPNN and ResNet models. Maps were generated using ArcGIS Desktop 10.6.1 (Build 9270, https://www.esri.com).

5.4. Model area generalizability

Tibet's complex geological and climatic conditions result in distinct differences in landslide development mechanisms and distribution patterns across different regions. For instance, within the Yarlung Zangbo River basin, 53.4% of landslides are concentrated along the main channel suture zone, while 62.6% occur in interbedded soft and hard rock

formations. River lateral erosion and stratigraphic lithology are the dominant factors influencing landslide occurrence (Zhao and Su, 2025). In the Lhasa River basin, over 70% of landslides develop in soft rock formations such as shale and schist with low weathering resistance, significantly influenced by freeze-thaw cycles and engineering disturbances (Zhao et al., 2023). In the Three Parallel Rivers region, high-elevation rockfall-debris flow landslides and fault-controlled landslides account for over 95% of occurrences. Intense tectonic activity and steep canyon topography jointly determine the development pattern of landslides (Yang et al., 2024). The differences in landslide development mechanisms and distribution characteristics across study areas introduce strong spatial heterogeneity into the raw data.

Due to the spatial heterogeneity of the original data, landslide susceptibility assessment models must possess strong generalizability to deliver effective evaluations across regions with varying characteristics. To investigate the model's generalizability, five typical landslide-prone areas were selected from the study region, as shown in Figure 12.

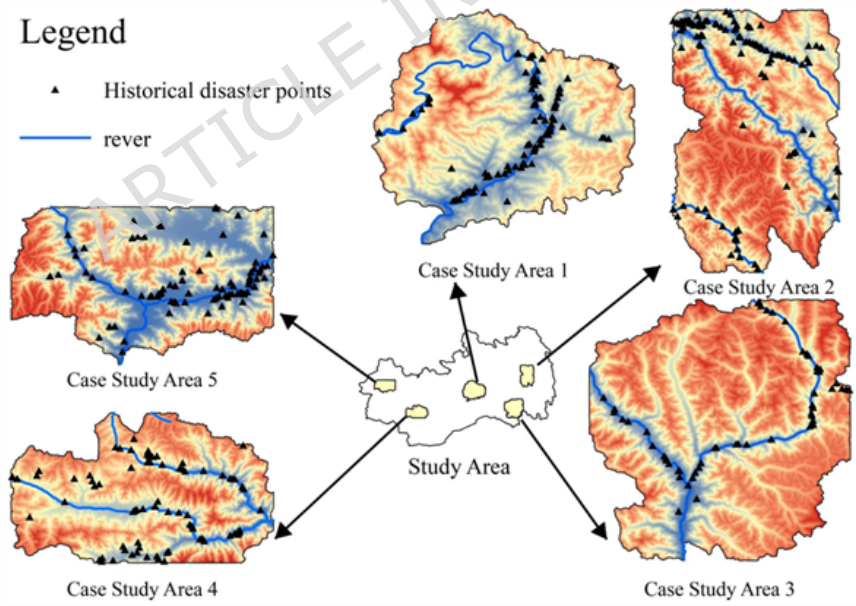

Figure 12: Typical landslide areas. Maps were generated using ArcGIS Desktop 10.6.1 (Build 9270, https://www.esri.com).

Within the typical areas, non-disaster site samples matching the number of historical disaster sites were randomly selected. ROC curves were plotted based on the evaluation results of the three models, and their AUC values were calculated.

Case Study Area 1 encompasses the Great Bend of the Yarlung Zangbo River in Medog and Milin counties, covering approximately 7,767.15 km². Characterized by extreme topography and severe river erosion, this area has recorded 103 historical disaster sites. The evaluation results of the three models are shown in Figure 13. In Case Study Area 1, the AUC values for the three models are 0.9230, 0.9045, and 0.8740. The physically constrained U-Net model performs best. The classification results of the three models are largely consistent, but the physically constrained U-Net model identifies a greater number of very high susceptibility zone.

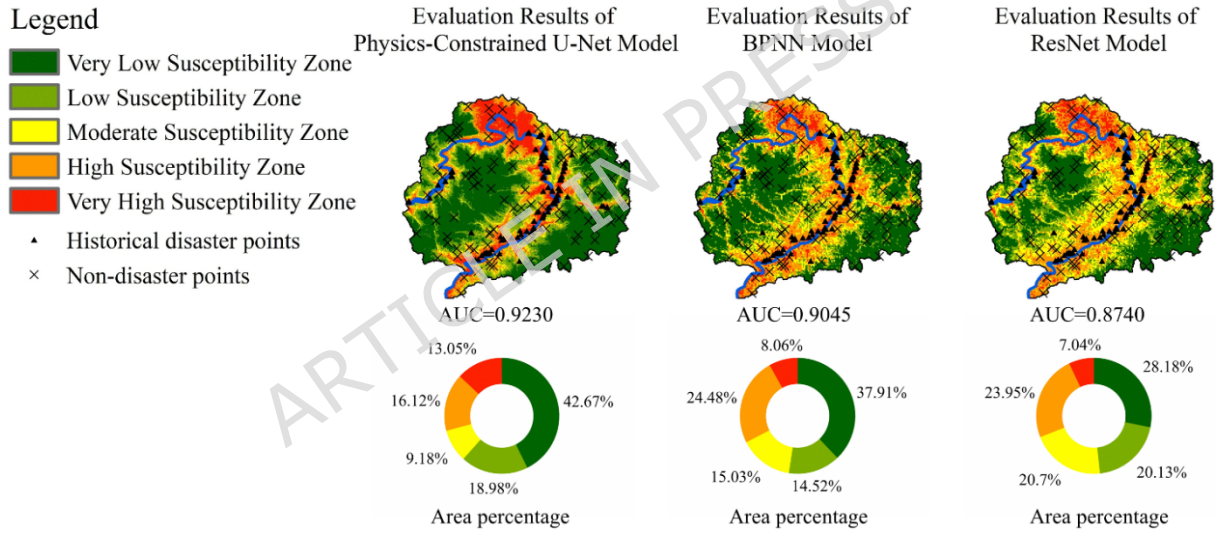

Figure 13: Evaluation Results of the Three Models in Case Study Area 1. Maps were generated using ArcGIS Desktop 10.6.1 (Build 9270, https://www.esri.com).

Case Study Area 2 is located within Chaya and Zogong counties, covering an area of approximately 6,063.14 km². It encompasses rivers such as the Lancang River, Shiqu River, and Weiqu River, characterized by deeply incised river valleys and fractured rock masses. A total of 107 historical disaster sites have been recorded within this area. The evaluation results of the three models are shown in Figure 14. In Case Study Area 2, the AUC values for the three models are 0.9403, 0.9295, and 0.9205. The physically constrained U-Net

model performs best. All three models classify the area near the river as a high susceptibility zone. The physically constrained U-Net model indicates that the region has virtually no very low susceptibility zone, underscoring the significant risk present in this area.

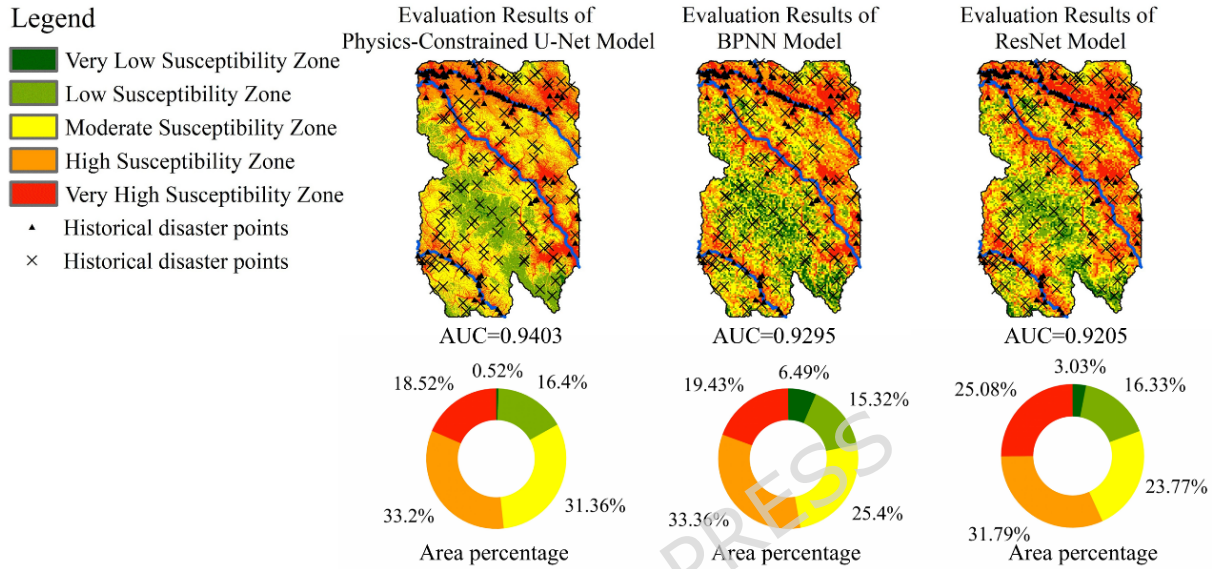

Figure 14: Evaluation Results of the Three Models in Case Study Area 2. Maps were generated using ArcGIS Desktop 10.6.1 (Build 9270, https://www.esri.com).

Case Study Area 3 is located in Chayu County, covering an area of approximately 7,134.03 km². It includes the Gongrigabu and Quluxite rivers, characterized by extensive glacial till deposits. Influenced by the East Himalayan tectonic structure, the area exhibits well-developed faults and frequent seismic activity, with 53 historical disaster sites recorded. The evaluation results of the three models are shown in Figure 15. In Case Study Area 3, the AUC values for the three models are 0.9345, 0.8708, and 0.9153. The physically constrained U-Net model performs best. The differences among the three model classification results primarily lie in moderate susceptibility zone. The physically constrained U-Net model indicates that landslide susceptibility risks in this region are more concentrated.

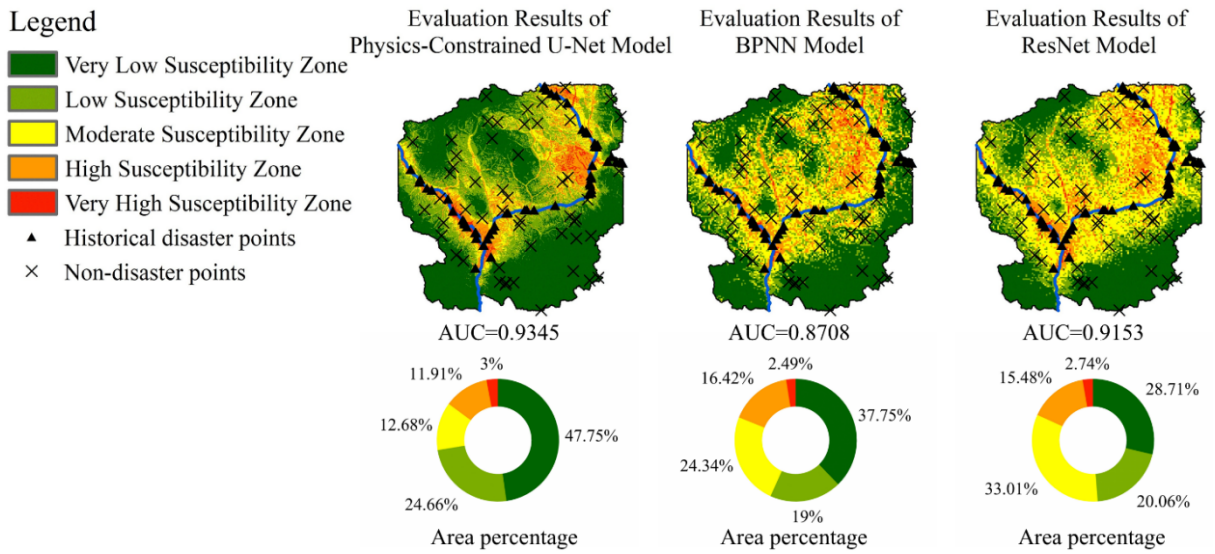

Figure 15: Evaluation Results of the Three Models in Case Study Area 3. Maps were generated using ArcGIS Desktop 10.6.1 (Build 9270, https://www.esri.com).

Case Study Area 4 spans Longzi and Cuona counties, covering approximately 5,380.47 km². It includes rivers such as the Jiaboqu and Longzixongqu, situated on the northern foothills of the Himalayas. The area experiences intense freeze-thaw cycles and severe glacial retreat, with 81 historical disaster sites recorded. The evaluation results of the three models are shown in Figure 16. In Case Study Area 4, the AUC values for the three models are 0.9150, 0.8768, and 0.8912. The physically constrained U-Net model performs best. It identified the fewest very low susceptibility zones.

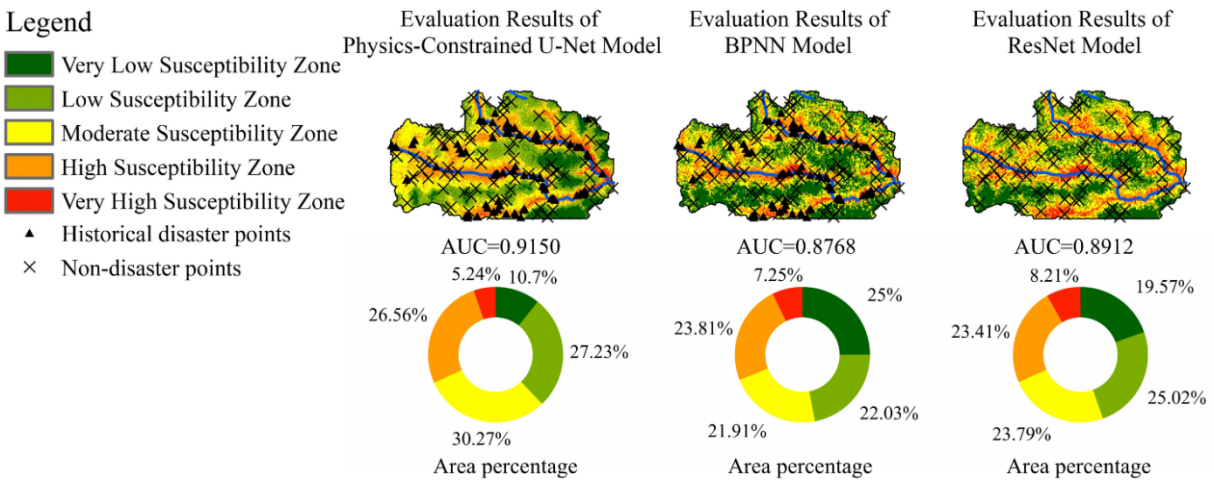

Figure 16: Evaluation Results of the Three Models in Case Study Area 4. Maps were generated using ArcGIS Desktop 10.6.1 (Build 9270, https://www.esri.com).

Case Study Area 5 is located in Lhasa, covering approximately 5,163.22 km². It includes rivers such as the Dielong River and the Lhasa River. Human activity has significantly impacted this area, and severe weathering occurs. A total of 87 historical disaster sites has been recorded. The evaluation results of the three models are shown in Figure 17. In Case Study Area 5, the AUC values for the three models are 0.8987, 0.9198, and 0.9135. The BP neural network model performs best, while the physically constrained U-Net model still demonstrated good accuracy. Their assessments of high-risk areas are largely consistent.

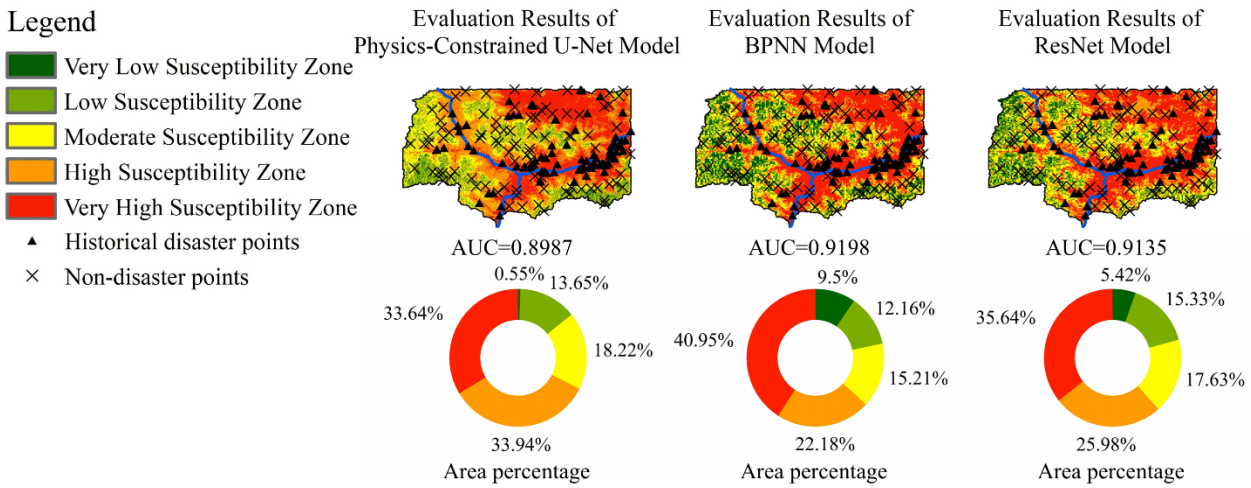

Figure 17: Evaluation Results of the Three Models in Case Study Area 5. Maps were generated using ArcGIS Desktop 10.6.1 (Build 9270, https://www.esri.com).

The physically constrained U-Net model outperformed both the BP neural network model and the residual neural network model in typical regions 1 to 4. Even in the relatively challenging typical region 5, its AUC value reached 0.90. The physically constrained U-Net model demonstrated robust performance across all typical zones, proving its effectiveness in assessing susceptibility across regions with diverse landslide development mechanisms and characteristics. This indicates strong generalization capabilities, enabling it to effectively address spatial heterogeneity in raw data.

5.5. Limitations and future directions

The data used in this paper are obtained from open-source websites, which have certain limitations in terms of accuracy and timeliness. In addition, due to the large scope of the study and limitations in research conditions, this study did not conduct field investigations. In future research, representative areas can be selected to obtain detailed geological data through field investigations, and more detailed and complex physical models can be constructed to impose stronger constraints on the U-Net model, thereby further improving the model's generalization capability. In addition, the handling of issues such as data imbalance should not be limited to adjusting the model itself. More data

augmentation and sampling methods can be explored to refine the dataset, improve data quality, and further enhance the accuracy of the evaluation results.

6. Conclusion

This study employs a U-Net model with definite physical constraints for landslide susceptibility assessment and compares it with BPNN and ResNet methods, yielding the following conclusions:

(1) Traditional neural network landslide susceptibility assessment methods retain whole features while progressively discarding spatial detail features, resulting in final assessment outcomes with low spatial resolution. The skip-connection structure inherent to the U-Net model enables it to preserve the spatial detail features of landslide assessment factors. This ultimately yields high-resolution landslide susceptibility assessments with the same spatial resolution as the assessment factors, better revealing the spatial characteristics of landslide hazard distribution and demonstrating greater precision.

(2) As an emerging data-driven approach, deep learning still suffers from two fundamental issues: it is highly susceptible to raw data and places excessive emphasis on numerical correlations while neglecting physical relationships. To address this, this paper adjusts the weights assigned to landslide and non-landslide samples within the cross-entropy function. By constraining the loss function based on a landslide early warning system, the approach ensures the model thoroughly learns both landslide and non-landslide features while penalizing unreasonable prediction behaviors. Finally, the model's evaluation results showed that the AUC value increased from 0.871 to 0.877, the recall increased from 0.884 to 0.891, and the Kappa coefficient increased from 0.597 to 0.605. Meanwhile, the frequency ratio of the very high susceptibility zone increased from 5.64 to 5.80, while that of the very low susceptibility zone decreased from 4.77×10^{-2} to 3.23×10^{-2}. This indicates that the weight adjustment and physical constraints imposed on the model's loss function have effectively improved the model's performance.

(3) The spatial heterogeneity of landslide distribution necessitates that landslide susceptibility assessment models possess strong generalizability. This study selected five

typical landslide-prone areas to evaluate model performance across regions with varying landslide development mechanisms and distribution characteristics, comparing the results with other deep learning models. The BP neural network model performed poorly in typical regions 2 and 3, while the residual neural network model showed poor performance in typical region 1. However, the physically constrained U-Net model achieved relatively high accuracy in all five regions, with AUC values of 0.923, 0.940, 0.935, 0.915, and 0.899, respectively. This confirms its robust generalizability and ability to effectively address spatial heterogeneity.

Conflict of interests

The authors declare no conflicts of interests.

Funding

This research was supported by the Second Tibetan Plateau Scientific Expedition and Research Program (STEP), Grant No.2019QZKK0906-02.

Authors' contributions

H.Z.: Theoretical analysis, Experiments, Writing - review & editing; H.D.: Conceptualization, Theoretical analysis, Experiments, Review

Data Availability

Hardware: CPU: 13th Gen Intel(R) Core (TM) i7-13700KF; RAM: 32 GB; GPU: NVIDIA GeForce RTX 3080.

Program language: Python

The data used in this study are listed in Table 1. The evaluation results are available for downloading at the link: https://doi.org/10.6084/m9.figshare.30741809

Code Availability

Hardware: CPU: 13th Gen Intel(R) Core (TM) i7-13700KF; RAM: 32 GB; GPU: NVIDIA GeForce RTX 3080.

Program language: Python

The source codes are available for downloading at the link:

https://doi.org/10.6084/m9.figshare.30741809

References

Brabb, E. E. (1991). The world landslide problem. Episodes, 14(1), 52-61.

Chen, W., Li, X., Wang, Y., Hong, H., & Pham, B. T. (2019). Comparison of convolutional neural networks for landslide susceptibility mapping in Yanshan County, China. Science of The Total Environment, *666*, 975-993. https://doi.org/10.1016/j.scitotenv.2019.02.263

Ciurleo, M., Cascini, L., & Calvello, M. (2017). A comparison of statistical and deterministic methods for shallow landslide susceptibility zoning in clayey soils. Engineering Geology, *223*, 71-81. https://doi.org/10.1016/j.enggeo.2017.04.023

Duan, Y., Ding, M., He, Y., Zheng, H., Delgado-Téllez, R., Sokratov, S., Dourado, F., & Fuchs, S. (2025). Global projections of future landslide susceptibility under climate change. Geoscience Frontiers, *16*, 102074. https://doi.org/10.1016/j.gsf.2025.102074

Emberson, R., Kirschbaum, D., & Stanley, T. (2020). New global characterisation of landslide exposure. Natural Hazards and Earth System Sciences, *20*, 3413-3424. https://doi.org/10.5194/nhess-20-3413-2020

Frattini, P., Crosta, G., & Carrara, A. (2010). Techniques for evaluating the performance of landslide susceptibility models. Engineering Geology, *111*(1-2), 62-72. https://doi.org/10.1016/j.enggeo.2009.12.004

Guzzetti, F., Rossi, M., & Salvati, P. (2020). Geographical landslide early warning systems. Earth-Science Reviews, *200*, 102973. https://doi.org/10.1016/j.earscirev.2019.102973

Gupta, S. K., & Shukla, D. P. (2023). Handling data imbalance in machine learning based landslide susceptibility mapping: a case study of Mandakini River Basin, North-Western Himalayas. Landslides, *20*, 933-949. https://doi.org/10.1007/s10346-022-01998-1

Han, Y., & Semnani, S. J. (2025). Important considerations in machine learning-based landslide susceptibility assessment under future climate conditions. Acta Geotechnica, *20*(2), 475–500. https://doi.org/10.1007/s11440-024-02396-8

He, R., Zhang, W., Dou, J., Jiang, N., Xiao, H., & Zhou, J. (2024). Application of artificial intelligence in three aspects of landslide risk assessment: A comprehensive review. Rock Mechanics Bulletin, *3*(4), 100144. https://doi.org/10.1016/j.rockmb.2024.100144

Hong, H., Wang, D., Zhu, A.-X., & Wang, Y. (2024). Landslide susceptibility mapping based on the reliability of landslide and non-landslide sample. Expert Systems with Applications, *243*, 122933. https://doi.org/10.1016/j.eswa.2023.122933

Hong, H. (2023). Landslide susceptibility assessment using locally weighted learning integrated with machine learning algorithms. Expert Systems with Applications, *234*, 121678. https://doi.org/10.1016/j.eswa.2023.121678

Hong, H. (2023). Assessing landslide susceptibility based on hybrid multilayer perceptron with ensemble learning. Bulletin of Engineering Geology and the Environment, *82*(10), 382. https://doi.org/10.1007/s10064-023-03409-8

Huang, F., et al. (2024). Modelling landslide susceptibility prediction: A review and construction of semi-supervised imbalanced theory. Earth-Science Reviews, *250*, 104700. https://doi.org/10.1016/j.earscirev.2024.104700

Huang, W., et al. (2023). Landslide susceptibility mapping and dynamic response along the Sichuan-Tibet transportation corridor using deep learning algorithms. CATENA, *222*, 106866. https://doi.org/10.1016/j.catena.2022.106866

Huang, Y., & Zhao, L. (2018). Review on landslide susceptibility mapping using support vector machines. Catena, *165*, 520-529. https://doi.org/10.1016/j.catena.2018.03.003

Jiang, Y., Wang, W., Zou, L., Cao, Y., & Xie, W.-C. (2025). Investigating landslide data balancing for susceptibility mapping using generative and machine learning models. Landslides, *22*, 189–204. https://doi.org/10.1007/s10346-024-02352-3

Kong, L., Feng, W., Yi, X., Xue, Z., & Bai, L. (2025). Enhanced landslide susceptibility mapping in data-scarce regions via unsupervised few-shot learning. Gondwana Research, *138*, 31-46. https://doi.org/10.1016/j.gr.2024.10.011

Li, J., Zhou, Z., & Ma, W. (2025). Assessment of landslide susceptibility along the Lanzhou-Xinjiang high-speed railway: A case study of Menyuan-Shandanmachang. Transportation Geotechnics, *50*, 101473. https://doi.org/10.1016/j.trgeo.2024.101473

Lin, Q., Steger, S., Pittore, M., Zhang, J., Wang, L., Jiang, T., & Wang, Y. (2022). Evaluation of potential changes in landslide susceptibility and landslide occurrence frequency in China under climate change. Science of the Total Environment, *850*, 158049. https://doi.org/10.1016/j.scitotenv.2022.158049

Petley, D. (2012). Global patterns of loss of life from landslides. Geology, 40(10), 927-930. https://doi.org/10.1130/G33217.1

Piciullo, L., Calvello, M., & Cepeda, J. M. (2018). Territorial early warning systems for rainfall- induced landslides. *Earth-Science Reviews, 179*, 228-247. https://doi.org/10.1016/j.earscirev.2018.02.001

Qian, L., Ou, L., Li, G., Chen, Y., & Qian, B. (2025). Optimizing the application of machine learning models in predicting landslide susceptibility using the information value model in Junlian County of Sichuan Basin. Advances in Space Research, *76*(2), 699-717. https://doi.org/10.1016/j.asr.2025.05.020

Reichenbach, P., Rossi, M., Malamud, B. D., Mihir, M., & Guzzetti, F. (2018). A review of statistically-based landslide susceptibility models. Earth-Science Reviews, *180*, 60-91. https://doi.org/10.1016/j.earscirev.2018.03.001

Shi, Q., Xu, X., Li, J., Deng, H., Zhang, Q., Tan, D., & He, Y. (2025). Spatiotemporal effect driven landslide susceptibility mapping at fine scales: a deep learning model based on multidimensional feature fusion and source data adaptation. Engineering Applications of Artificial Intelligence, *156*, 110924. https://doi.org/10.1016/j.engappai.2025.110924

Sun, H., Li, W., Scaloni, M., Fu, J., Guo, X., & Gao, J. (2023). Influence of spatial heterogeneity on landslide susceptibility in the transboundary area of the Himalayas. Geomorphology, *433*, 108723. https://doi.org/10.1016/j.geomorph.2023.108723

Su, Y., Fu, J., Lai, X., Lin, C., Zhu, L., Xie, X., Jiang, J., Chen, Y., Huang, J., & Huang, W. (2025). Complex cross-regional landslide susceptibility mapping by multi-source domain

transfer learning. Geoscience Frontiers, 102053. https://doi.org/10.1016/j.gsf.2025.102053

Tsangaratos, P., Ilia, I., Hong, H., Chen, W., & Xu, C. (2020). Comparing the prediction performance of a Deep Learning Neural Network model with conventional machine learning models in landslide susceptibility assessment. CATENA, *188*, 104426. https://doi.org/10.1016/j.catena.2019.104426

Wang, H., Zhang, L., Luo, H., He, J., & Cheung, R. W. M. (2021). AI-powered landslide susceptibility assessment in Hong Kong. Engineering Geology, *288*, 106103. https://doi.org/10.1016/j.enggeo.2021.106103

Wang, H., Wang, L., & Zhang, L. (2022). Transfer learning improves landslide susceptibility assessment. Gondwana Research, 123, 238-254. https://doi.org/10.1016/j.gr.2022.07.008

Wang, Y., Zhang, W., Wang, L., Liu, S., Zhang, K., Liu, P., Sun, W., & Jiang, S. (2025). Cross-regional extrapolation of landslide susceptibility mapping via transfer learning. Geoscience Frontiers, 102212. https://doi.org/10.1016/j.gsf.2025.102212

Wang, Y., Wang, L., Liu, S., Han, L., Zhang, W., Hong, L., Zhu, Z., & Zhu, X. (2025). Region similarity assessment for empowering physics-informed transfer learning-based landslide susceptibility mapping. Journal of Rock Mechanics and Geotechnical Engineering. https://doi.org/10.1016/j.jrmge.2025.06.030

Wang, Y., Wang, L., Zhang, W., Liu, S., Sun, W., Hong, L., & Zhu, Z. (2024). A physics-informed machine learning solution for landslide susceptibility mapping based on three-dimensional slope stability evaluation. Journal of Central South University, 31(11), 3838-3853. https://doi.org/10.1007/s11771-024-5687-3

Wei, X., Zhang, L., Luo, J., & Liu, D. (2021). A hybrid framework integrating physical model and convolutional neural network for regional landslide susceptibility mapping. Natural Hazards, *109*(1), 471–497. https://doi.org/10.1007/s11069-021-04844-0

Yang, Z., Pang, B., Dong, W., Li, D., & Huang, Z. (2024). Interaction of landslide spatial patterns and river canyon landforms: Insights into the Three Parallel Rivers Area,

southeastern Tibetan Plateau. Science of The Total Environment, *914*, 169935. https://doi.org/10.1016/j.scitotenv.2024.169935

Zhao, B., & Su, L. (2025). Complex spatial and size distributions of landslides in the Yarlung Tsangpo River (YTR) basin. Journal of Rock Mechanics and Geotechnical Engineering, *17*(2), 897-914. https://doi.org/10.1016/j.jrmge.2024.01.021

Zhao, S., Dai, F., Deng, J., Wen, H., Li, H., & Chen, F. (2023). Insights into landslide development and susceptibility in extremely complex alpine geoenvironments along the western Sichuan–Tibet Engineering Corridor, China. CATENA, *227*, 107105. https://doi.org/10.1016/j.catena.2023.107105

Zhao, Z., Xu, Z., Hu, C., Wang, Q., & Ding, X. (2024). Geographically weighted neural network considering spatial heterogeneity for landslide susceptibility mapping: A case study of Yichang City, China. CATENA, *234*, 107590. https://doi.org/10.1016/j.catena.2023.107590

Zhong, L., Guo, Z., Qi, S., Zhao, T., Wu, B., & Li, P. (2024). Landslide susceptibility evaluation and determination of critical influencing factors in eastern Sichuan mountainous area, China. Ecological Indicators, *169*, 112911. https://doi.org/10.1016/j.ecolind.2024.112911

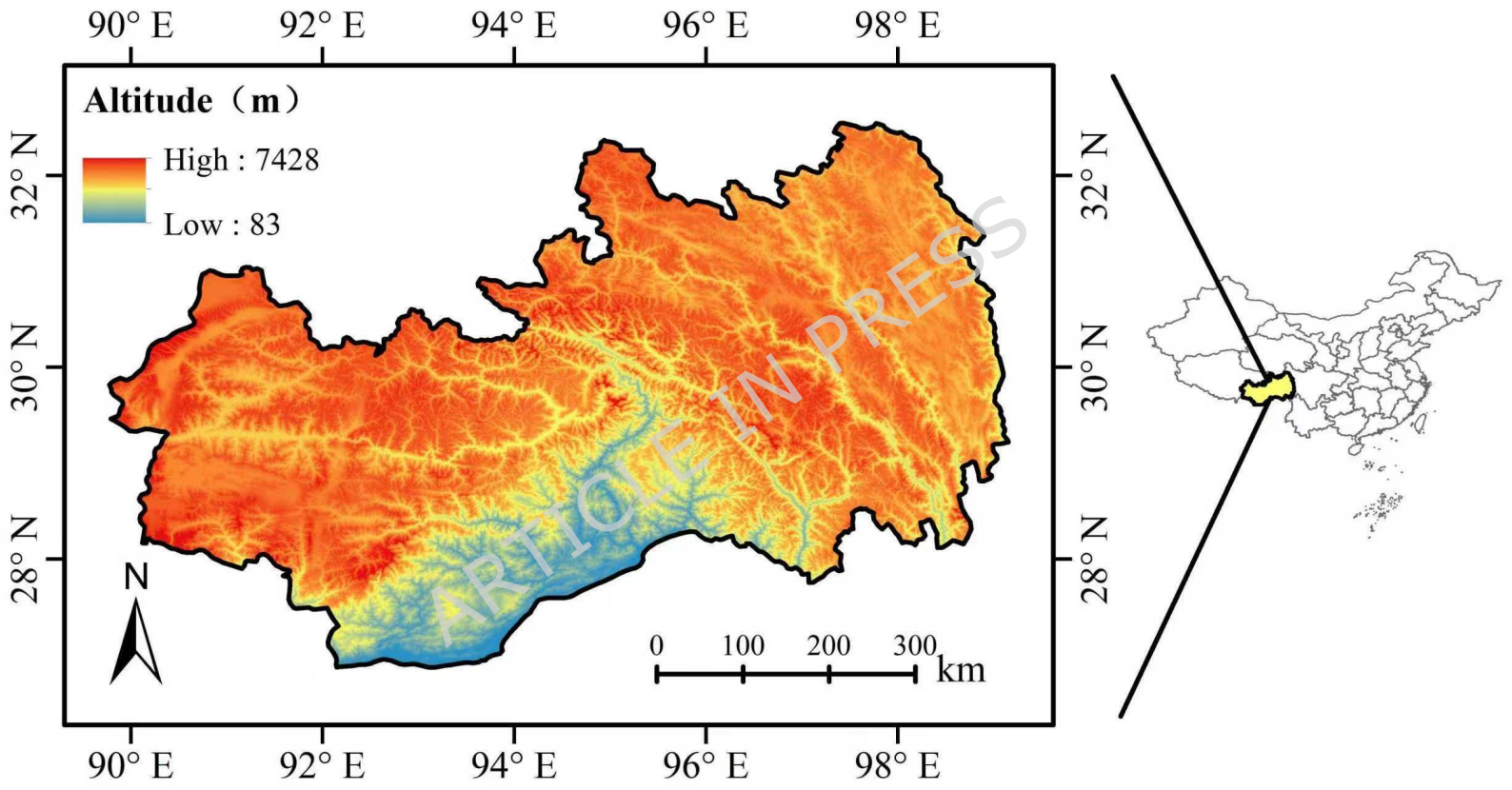

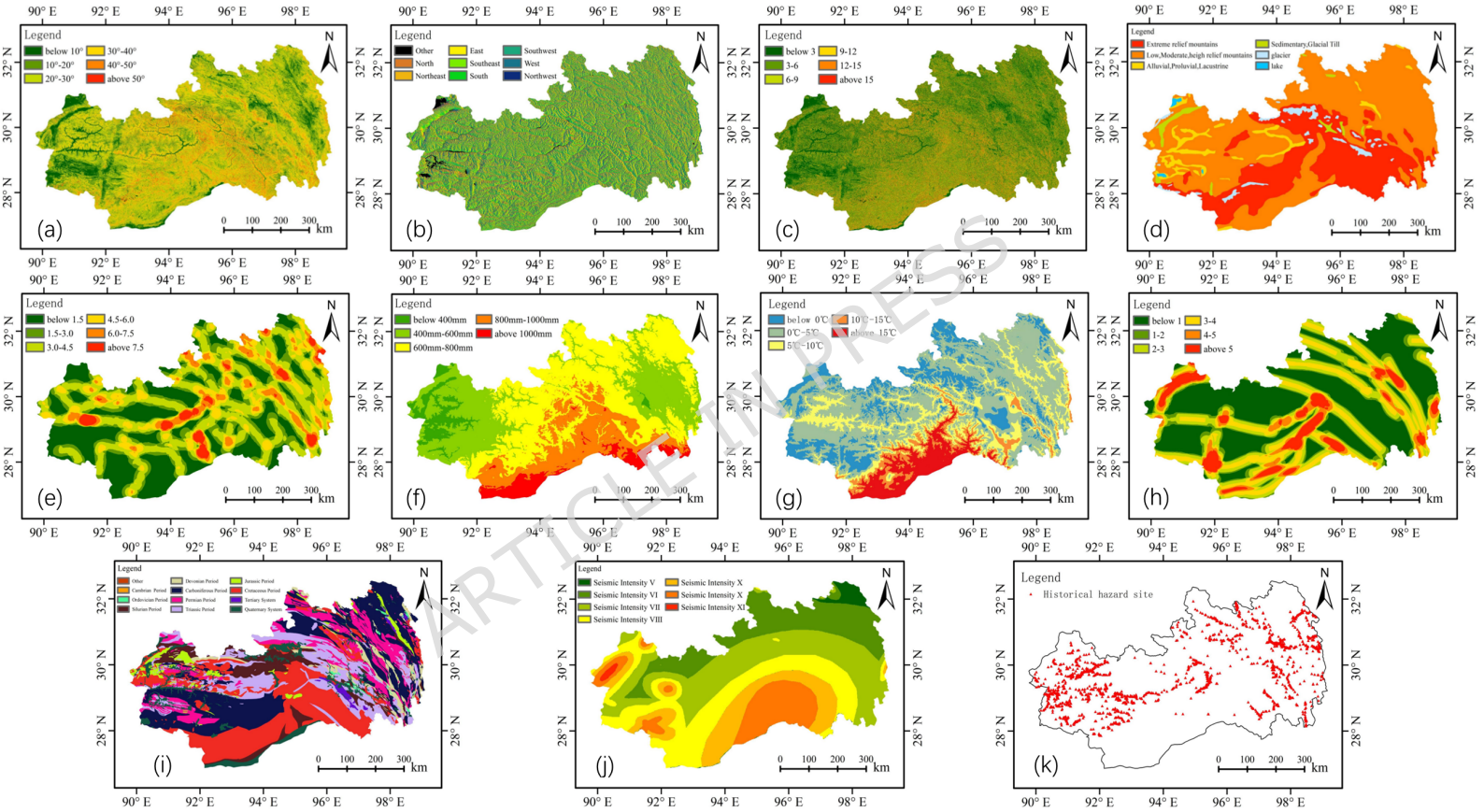

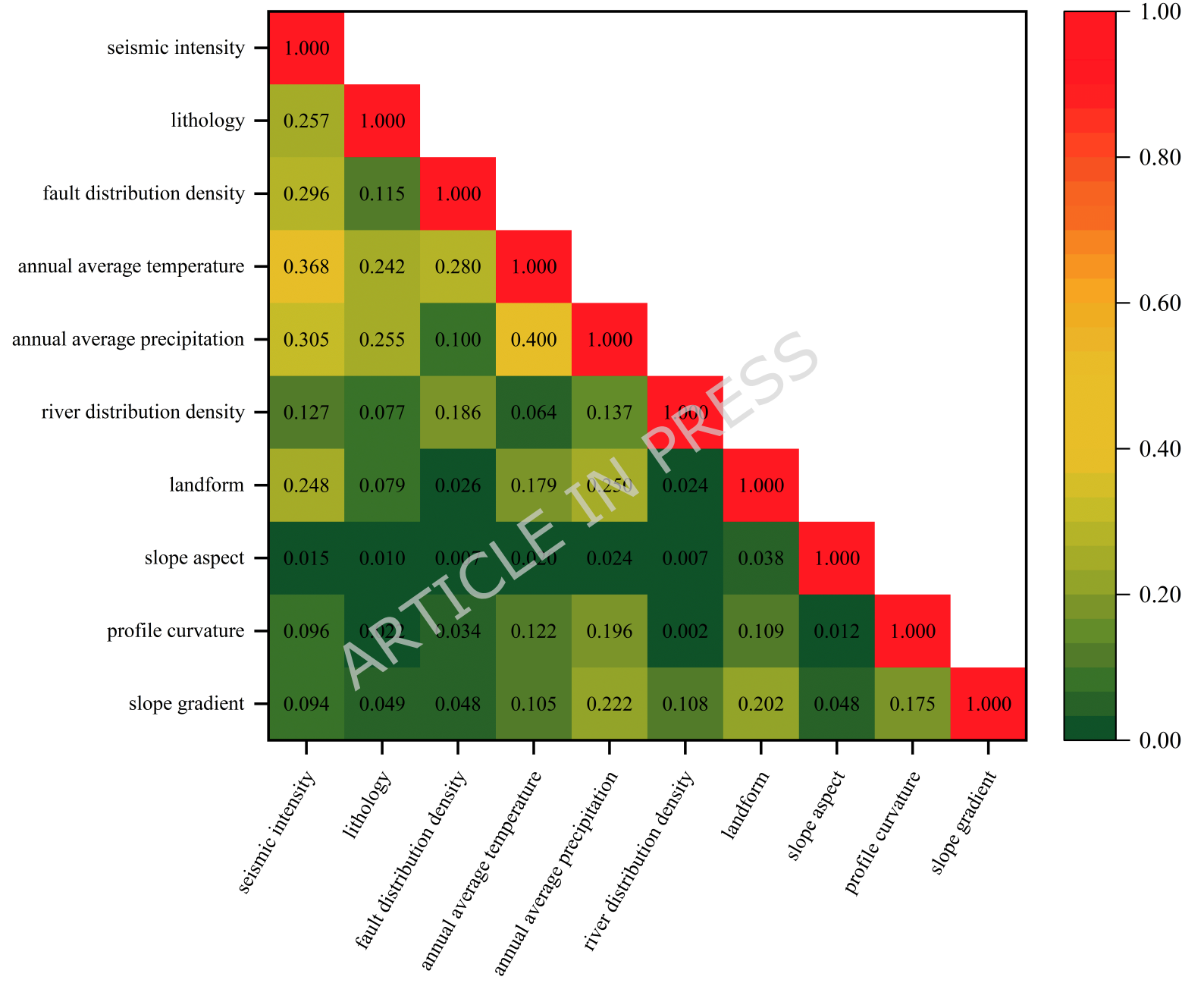

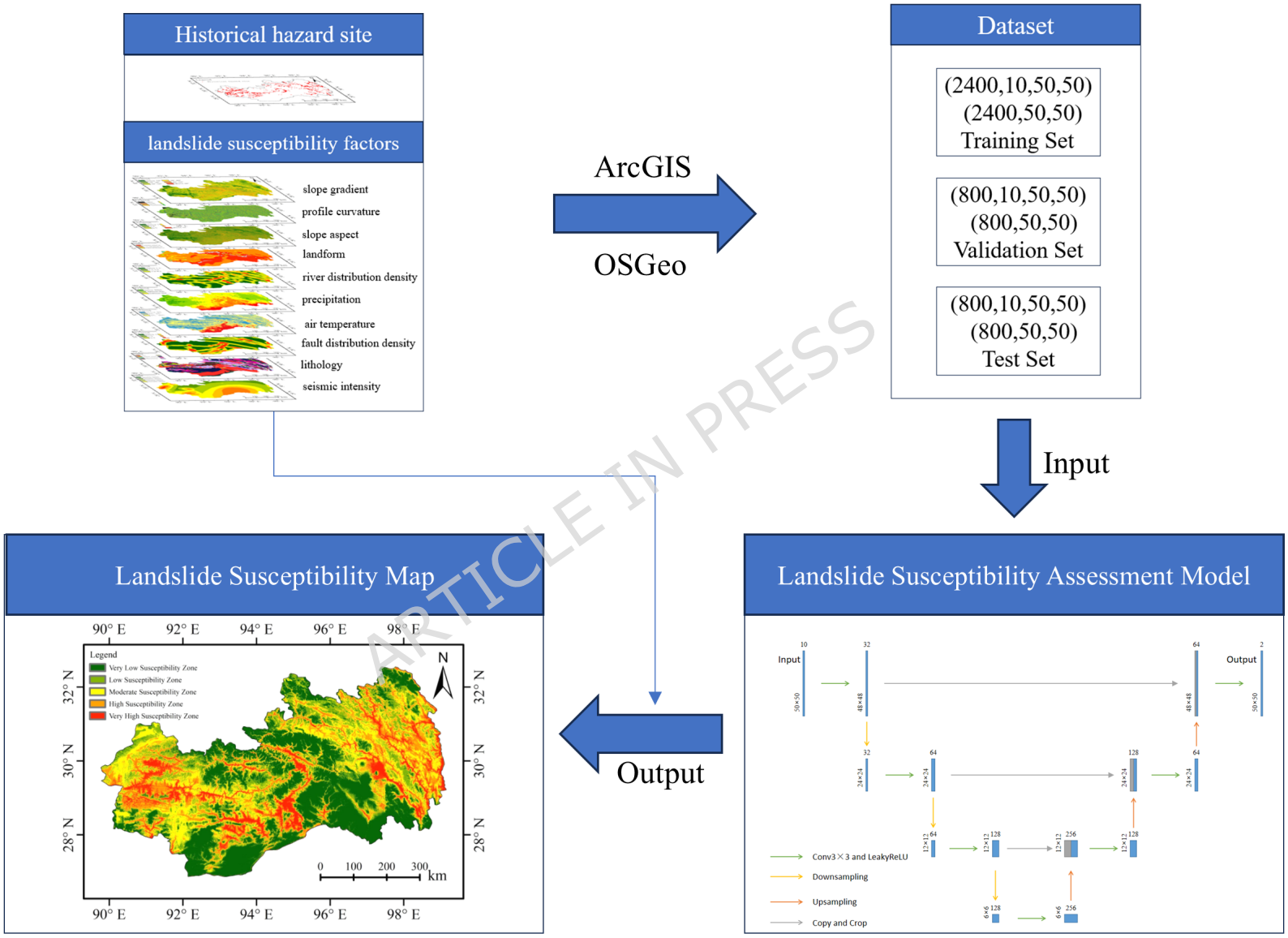

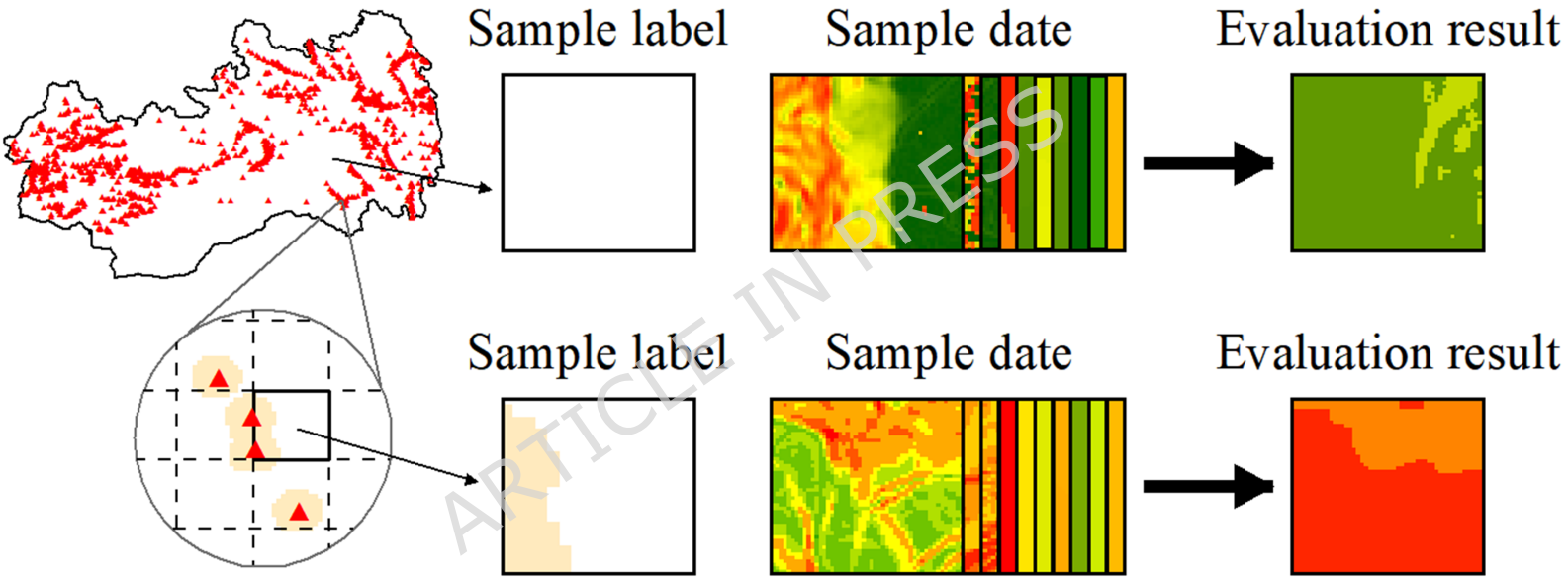

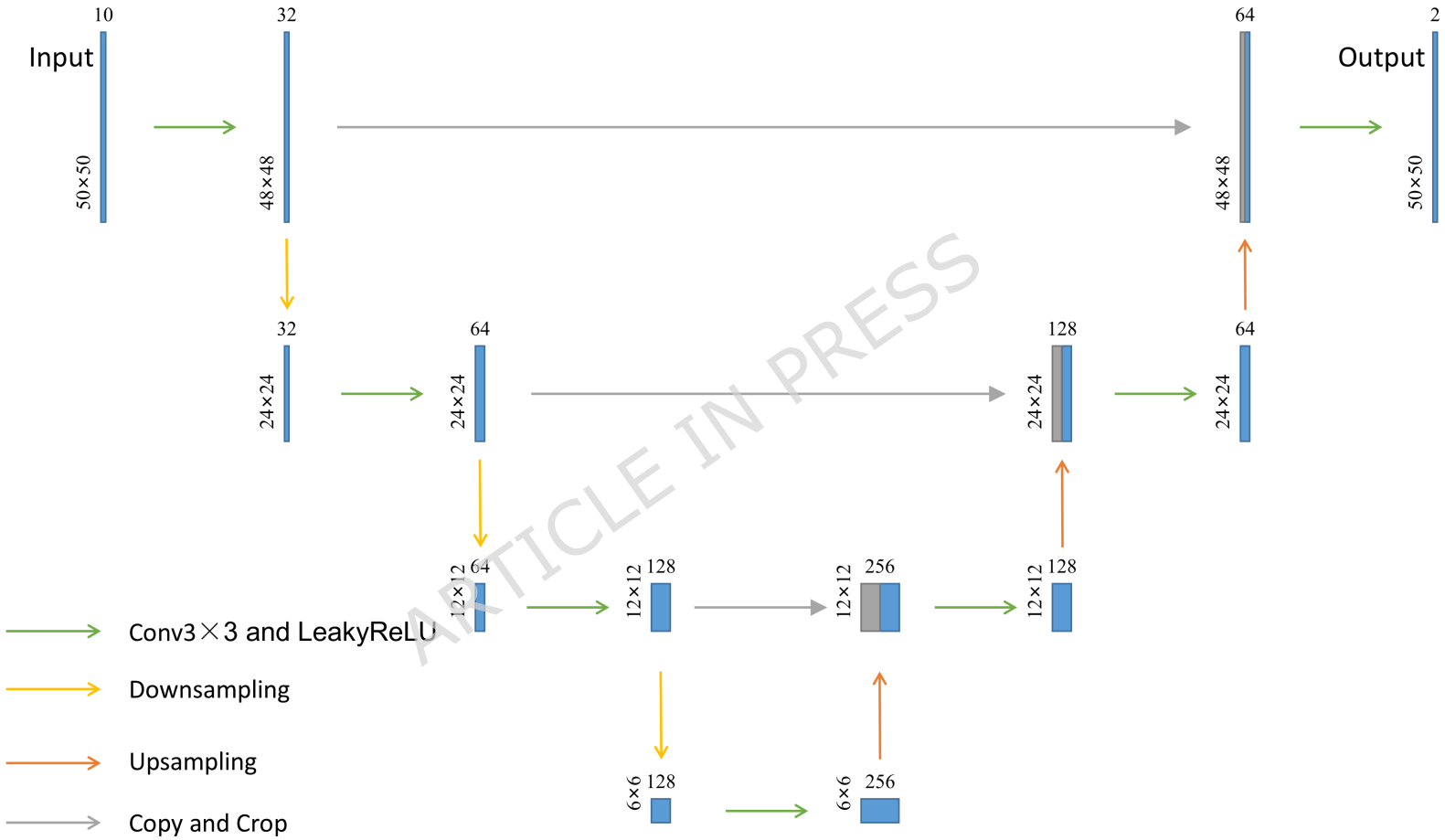

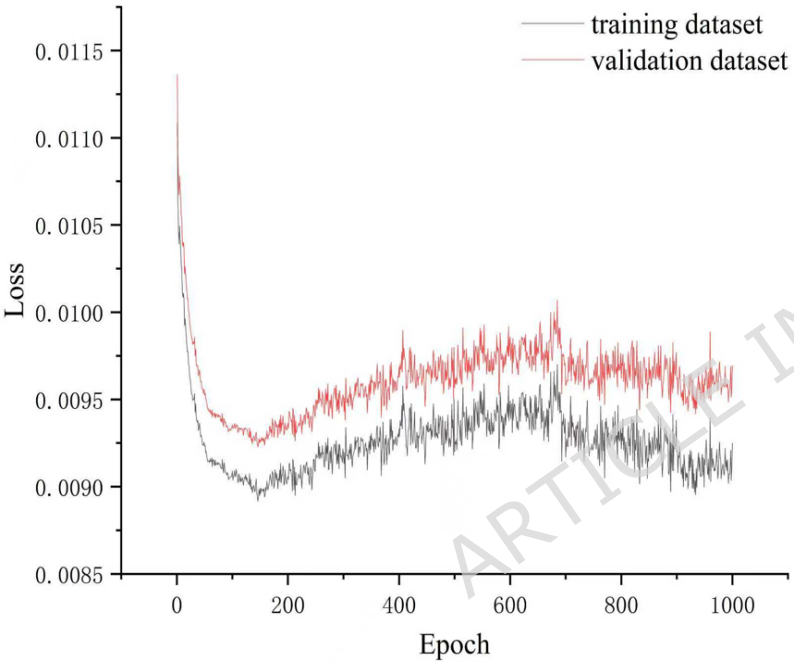

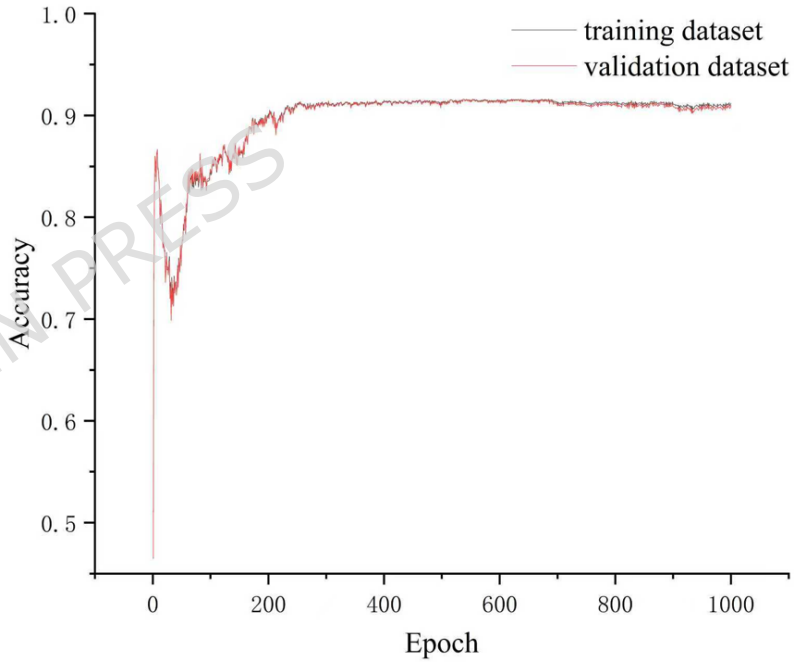

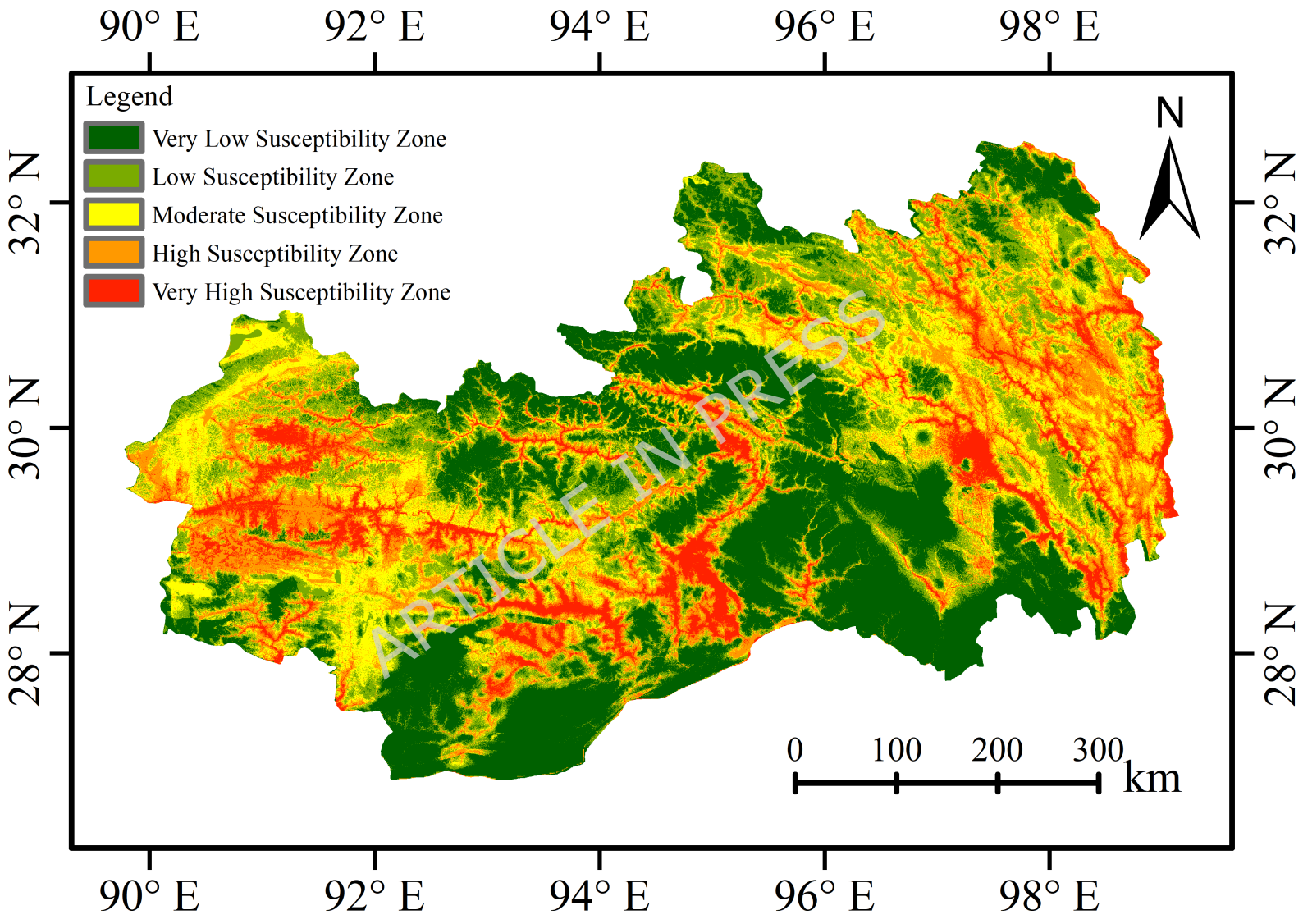

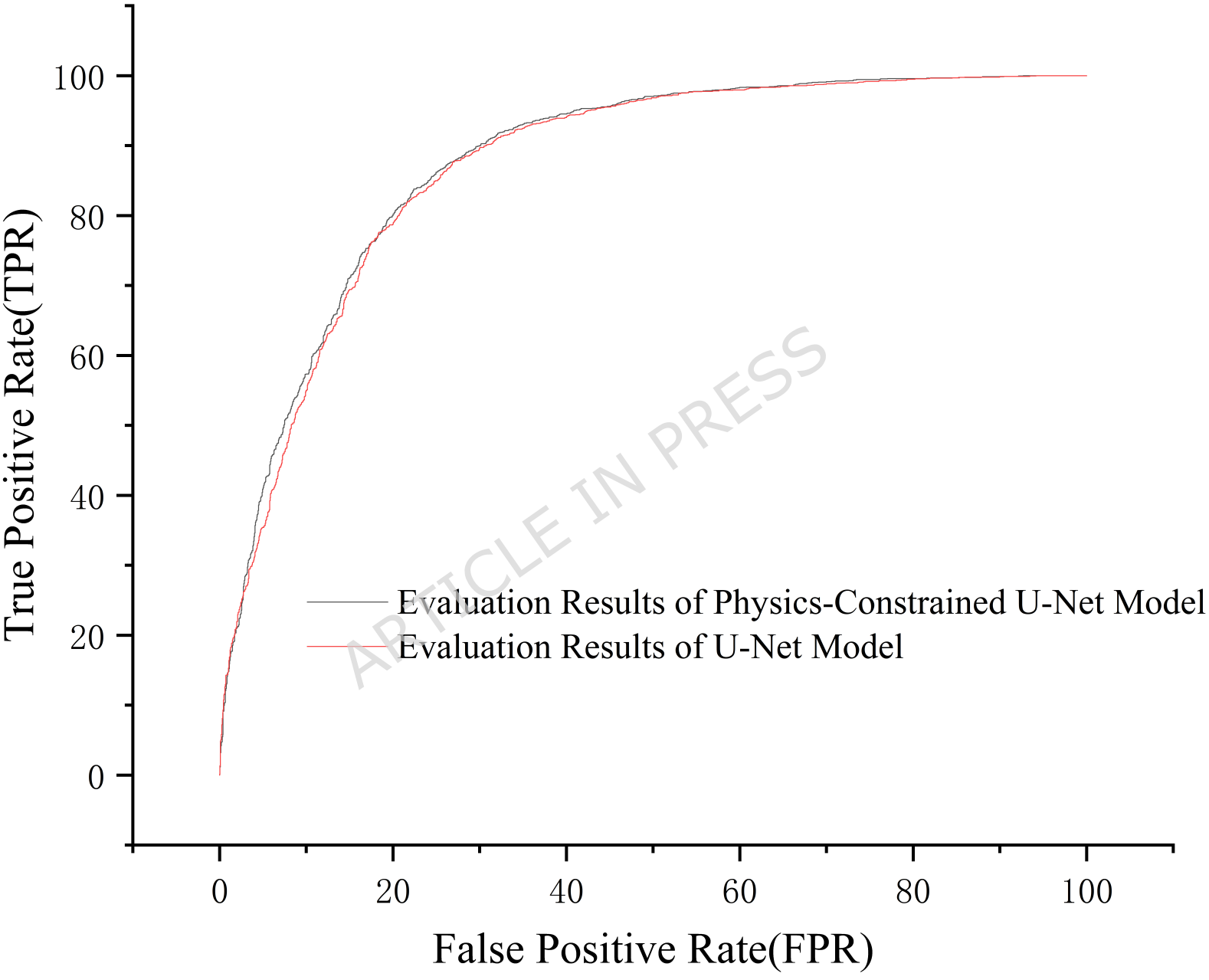

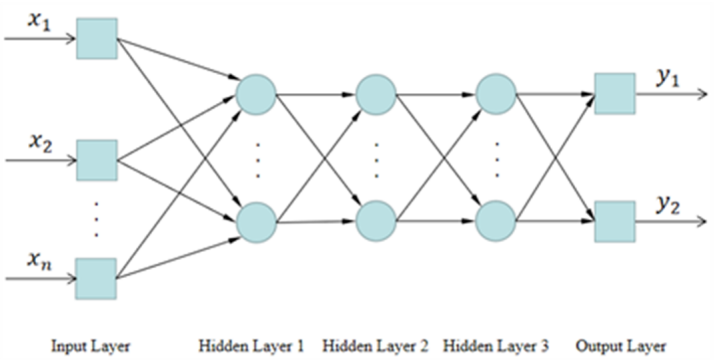

(a)

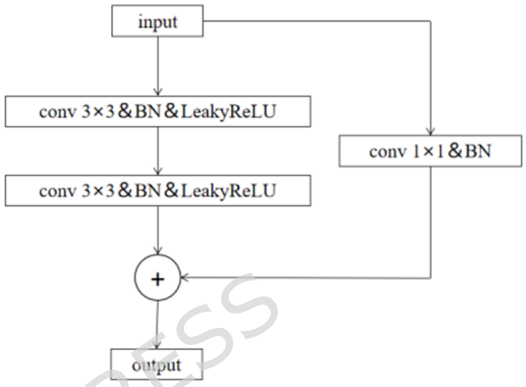

(b)

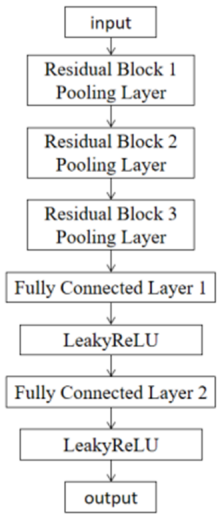

Residual Block ResNet

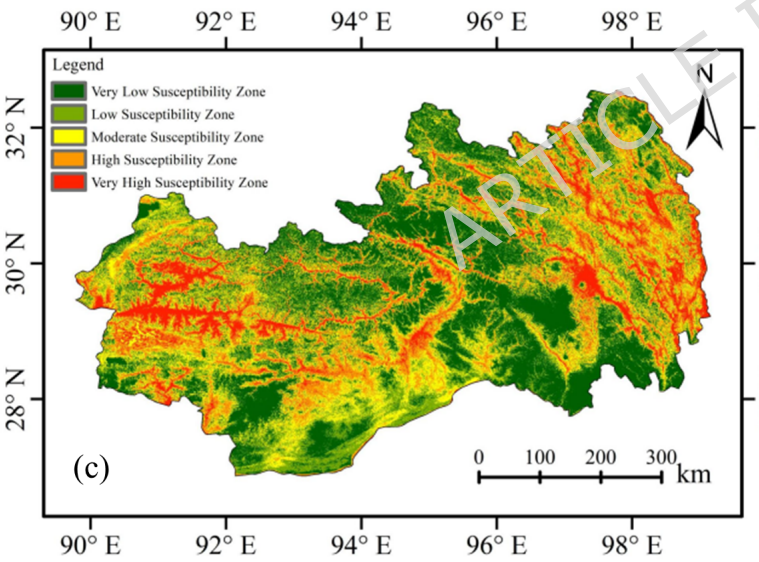

(c)

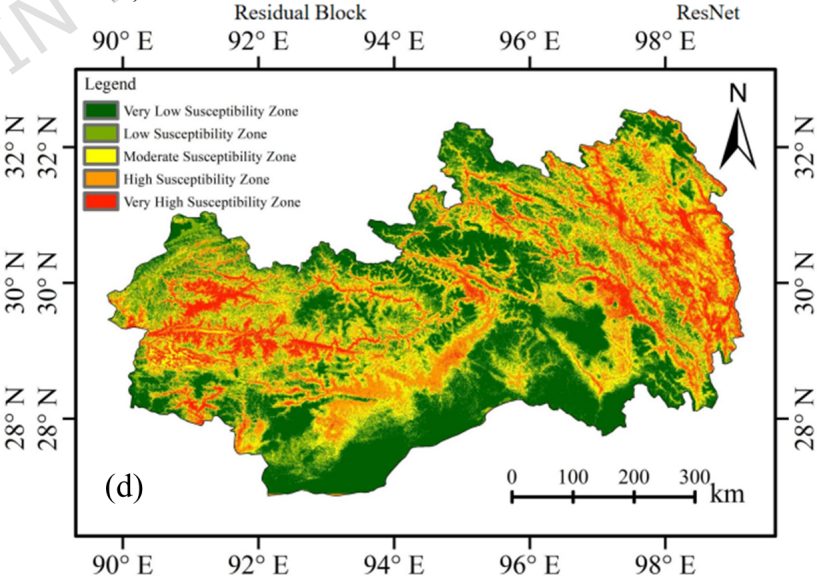

(d)